Atmos. Chem. Phys., 13, 7075–7095, 2013
www.atmos-chem-phys.net/13/7075/2013/
doi:10.5194/acp-13-7075-2013

Atmospheric Chemistry and Physics Open Access

Spatial and seasonal distribution of Arctic aerosols observed by the CALIOP satellite instrument (2006–2012)

M. Di Pierro[1], L. Jaeglé[1], E. W. Eloranta[2,3], and S. Sharma[4]

[1]Department of Atmospheric Sciences, University of Washington, Seattle, WA, USA
[2]Space Science and Engineering Center, University of Wisconsin, Madison, WI, USA
[3]Atmospheric and Oceanic Sciences Department, University of Wisconsin, Madison, WI, USA
[4]Environment Canada, Toronto, Ontario, Canada

Correspondence to: M. Di Pierro (dipierro@uw.edu)

Received: 21 December 2012 – Published in Atmos. Chem. Phys. Discuss.: 20 February 2013
Revised: 7 June 2013 – Accepted: 11 June 2013 – Published: 25 July 2013

Abstract. We use retrievals of aerosol extinction from the Cloud-Aerosol Lidar with Orthogonal Polarization (CALIOP) onboard the CALIPSO satellite to examine the vertical, horizontal and temporal variability of tropospheric Arctic aerosols during the period 2006–2012. We develop an empirical method that takes into account the difference in sensitivity between daytime and nighttime retrievals over the Arctic. Comparisons of the retrieved aerosol extinction to in situ measurements at Barrow (Alaska) and Alert (Canada) show that CALIOP reproduces the observed seasonal cycle and magnitude of surface aerosols to within 25 %. In the free troposphere, we find that daytime CALIOP retrievals will only detect the strongest aerosol haze events, as demonstrated by a comparison to aircraft measurements obtained during NASA's ARCTAS mission during April 2008. This leads to a systematic underestimate of the column aerosol optical depth by a factor of 2–10. However, when the CALIOP sensitivity threshold is applied to aircraft observations, we find that CALIOP reproduces in situ observations to within 20 % and captures the vertical profile of extinction over the Alaskan Arctic. Comparisons with the ground-based high spectral resolution lidar (HSRL) at Eureka, Canada, show that CALIOP and HSRL capture the evolution of the aerosol backscatter vertical distribution from winter to spring, but a quantitative comparison is inconclusive as the retrieved HSRL backscatter appears to overestimate in situ observations by a factor of 2 at all altitudes. In the High Arctic ($> 70°$ N) near the surface (< 2 km), CALIOP aerosol extinctions reach a maximum in December–March (10–20 Mm^{-1}), followed by a sharp decline and a minimum in May–September (1–4 Mm^{-1}), thus providing the first pan-Arctic view of Arctic haze seasonality. The European and Asian Arctic sectors display the highest wintertime extinctions, while the Atlantic sector is the cleanest. Over the Low Arctic (60–70° N) near the surface, CALIOP extinctions reach a maximum over land in summer due to boreal forest fires. During summer, we find that smoke aerosols reach higher altitudes (up to 4 km) over eastern Siberia and North America than over northern Eurasia, where they remain mostly confined below 2 km. In the free troposphere, the extinction maximum over the Arctic occurs in March–April at 2–5 km altitude and April–May at 5–8 km. This is consistent with transport from the midlatitudes associated with the annual maximum in cyclonic activity and blocking patterns in the Northern Hemisphere. A strong gradient in aerosol extinction is observed between 60° N and 70° N in the summer. This is likely due to efficient stratocumulus wet scavenging at high latitudes combined with the poleward retreat of the polar front. Interannual variability in the middle and upper troposphere is associated with biomass burning events (high extinctions observed by CALIOP in spring 2008 and summer 2010) and volcanic eruptions (Kasatochi in August 2008 and Sarychev in June 2009). CALIOP displays below-average extinctions observed from August 2009 through May 2010, which appear to be linked with a strongly negative Arctic Oscillation index.

Published by Copernicus Publications on behalf of the European Geosciences Union.

1 Introduction

Transport of anthropogenic aerosols to the Arctic has been studied since the early 1980s (e.g., Rahn and McCaffrey, 1980; Barrie et al., 1981; Rahn, 1981) and leads to the phenomenon of Arctic haze, the human-caused reduction in visibility at high latitudes. Arctic haze is characterized by a marked seasonal cycle in aerosol concentrations at the surface, with a maximum in winter/early spring and a minimum in summer (Law and Stohl, 2007; Quinn et al., 2007). The winter/spring maximum is due to enhanced transport combined with weaker removal in the Arctic (Shaw, 1995). The summer minimum has been attributed to the isolation of the Arctic atmosphere caused by reduced transport from midlatitudes at this time of year (e.g., Stohl, 2006), although recent studies have highlighted the importance of efficient summertime wet removal processes over the Arctic (Garrett et al., 2011; Bourgeois and Bey, 2011; Browse et al., 2012).

Considerable effort has been devoted to understanding the sources and transport pathways of Arctic pollution. Transport of pollution aerosols from Europe and the former Soviet Union (FSU) was the main source of Arctic aerosols in the 1980s (Rahn and Lowenthall, 1984; Raatz and Shaw, 1984; Barrie et al., 1989). However, since the first source-attribution studies were conducted, the geographical distribution of the emission of aerosols from fossil-fuel combustion has changed dramatically (Novakov et al., 2003). Sulfur emissions in eastern Europe and Russia have been decreasing following the introduction of cleaner combustion technologies in Europe and the demise of the FSU, whereas East and South Asian emissions have increased over the past 30 years, driven by rapid economic growth and higher energy consumption (Stern, 2005). Ground-based measurements of sulfate aerosol concentrations in March/April have decreased by 27–63 % between 1990 and 2003 across a range of Arctic sites, and appear to have leveled off (Quinn et al., 2007). This negative trend has been attributed to the decrease in anthropogenic emissions from Eurasia (Quinn et al., 2009; Gong et al., 2010); Hirdman et al., 2010). Recent modeling studies show that despite declining emissions, Europe and Russia continue to constitute the largest contributors of Arctic sulfate and black carbon (BC) aerosols at the surface (Shindell et al., 2008) due to their vicinity and favorable transport patterns to the Arctic (Stohl, 2006). Measurements of BC in snow across the Arctic (Hegg et al., 2010) as well as modeling simulations (Wang et al., 2011) suggest a large contribution from agricultural biomass burning during spring.

The 2008 International Polar Year (IPY) saw a suite of coordinated aircraft campaigns aimed at improving the understanding of the factors controlling changes in Arctic atmospheric composition and climate. The National Aeronautics and Space Administration (NASA) Arctic Research of the Composition of the Troposphere from Aircraft and Satellites (ARCTAS) campaign occurred in April (ARCTAS-A) and July (ARCTAS-B) of 2008 over the North American Arctic (Jacob et al., 2010). The spring campaign was conducted in parallel with the National Oceanic and Atmospheric Administration (NOAA) Aerosol Radiation and Cloud Processes affecting Arctic Climate (ARCPAC) campaign (Brock et al., 2011). During these springtime campaigns, several dense biomass burning plumes from agricultural and forest fires in Russia were sampled over the Alaskan and Canadian Arctic (Warneke et al., 2009; Fisher et al., 2010). Source attribution studies have determined that fossil-fuel burning in East Asia was the dominant source of pollution during ARCTAS-A, representing roughly 40 % of Arctic CO at all altitudes (Fisher et al., 2010; Bian et al., 2013), although European and Russian sources also contributed significantly at low altitudes (30 %). Wang et al. (2011) reported that sulfate aerosols contributed to 50–70 % of aerosol mass, with organic aerosols accounting for another 30–40 % at all altitudes. Fisher et al. (2011) found that the single largest source of sulfate aerosols at the surface is central Russia and Kazakhstan in winter–spring, whereas East Asia contributes the most above 5 km. The modeling study of Bourgeois and Bey (2011) indicates that Europe and Siberia dominate the annual budgets of column BC and sulfate aerosols. Biomass burning events systematically affect the springtime aerosol budgets and background concentration levels and April 2008 stands out as characterized by unusually high fire activity (Warneke et al., 2010). Brock et al. (2011) observed that the seasonality of Arctic haze is driven by changes in the background aerosols concentration rather than the frequency of occurrence of dense smoke layers.

The summer 2008 IPY measurements showed that the East Asian contribution to Arctic CO and aerosols was small, indicating inefficient transport as well as enhanced wet scavenging of aerosols (Matsui et al., 2011; Bian et al., 2013). Despite high plume dilution and stronger wet removal in summer, several aerosol plumes were traced to both fossil-fuel and biomass burning origins, and all showed a preponderant component of highly oxygenated organic carbon compounds (> 70 %) with relatively larger sulfate fractions for plumes originating in industrialized regions (Schmale et al., 2011).

In addition to fossil-fuel and biomass burning sources, the Arctic aerosol budget is also influenced by natural sources. Thin lofted layers of mineral dust were documented as early as the 1970s (Rahn et al., 1977). Greenland ice-core records spanning the recent past (1790–2000) show large spikes of deposited sulfate associated with episodic explosive volcanic eruptions (McConnell et al., 2007). These ice cores also show that biomass burning constitutes a significant, though highly variable, source in summer.

Pollution enters the Arctic following different pathways determined by the persistence and seasonality of large-scale circulation patterns. Carlson (1981) and Iversen (1984) introduced the concept of *polar dome*, a dome-shaped closely packed set of constant potential temperature surfaces (isentropes) wrapped around the Arctic. As transport within the Arctic tends to occur at near-constant potential temperature,

the polar dome forces air aloft to follow the isentropes, effectively acting as a surface barrier to intrusions of air from outside. However, during winter considerable diabatic cooling may occur in an air mass in contact with cold, snow-covered surfaces (Klonecki et al., 2003), thus trapping aerosols below the temperature inversion and allowing for their transport over long distances. This is a common low-level pollution transport pathway from Eurasia in winter and early spring.

Transport aloft requires that gaseous and aerosol pollutants first be injected from the planetary boundary layer into the free troposphere and is thus more episodic. Warm conveyor belts in midlatitude cyclones constitute such a mechanism, but are accompanied by considerable wet scavenging. Free-tropospheric transport via this pathway dominates the total transport from North America and East Asia because of the lower latitudes and higher potential temperatures of these regions compared to sources located in Europe and Russia (Klonecki et al., 2003; Stohl, 2006).

Although surface observations span more than three decades at a few sites such as Barrow (Alaska), Alert (Canada) and Karasjok (Norway), the Arctic aerosol burden is not well characterized in space and time (Quinn et al., 2007). Aircraft campaigns provide a snapshot of the detailed vertical distribution of Arctic aerosols, but only over a limited time period and region. For example, airborne measurements of aerosol properties were conducted during the Tropospheric Ozone Production about the Spring Equinox experiment (TOPSE) from February to May 2000 over the North American Arctic (Browell et al., 2003; Scheuer et al., 2003). The measurements highlighted the strong spatial inhomogeneity of Arctic aerosol mixing ratios and documented a steady increase in number concentration in the middle–upper troposphere throughout the campaign, providing indications that the annual aerosol maximum occurs later aloft than at the surface.

The SAGE II and III satellite instruments used solar occultation to retrieve aerosol extinction in the Arctic troposphere above 6 km altitude (Treffeisen et al., 2006). An April–May aerosol extinction maximum was observed in the upper troposphere, followed by a rapid drop in midsummer to much lower values. Thus SAGE provided the first multiyear dataset of Arctic aerosols in the upper troposphere. However, SAGE retrievals were not available in the middle and lower troposphere because of limitations associated with the presence of clouds along the long horizontal line of sight of the instrument.

The NASA and Centre National d'Études Spatiales (CNES) Cloud-Aerosol Lidar and Infrared Pathfinder Satellite Observation (CALIPSO) satellite joined the A-train polar-orbiting constellation on 28 April 2006 and began collecting data in June 2006 (Winker et al., 2009). CALIPSO carries the Cloud-Aerosol Lidar with Orthogonal Polarization (CALIOP) instrument, which measures the attenuated backscatter at 532 nm and 1064 nm with a vertical resolution of 30 to 60 m. Because it is an active remote sensing instrument, CALIOP can retrieve aerosol and cloud profile information during both daytime and nighttime, and, unlike passive remote sensing instruments, it is not affected by the highly reflective surfaces present in the Arctic. Thus, CALIOP has the potential to provide a wealth of information on the vertical and horizontal distribution of Arctic aerosols. Two limitations of CALIOP are its narrow footprint ($\sim$100 m) and its relatively low sensitivity to faint aerosol layers that frequently occur over the Arctic.

CALIPSO has been used in the Arctic to follow the evolution of aerosol plumes over timescales of 4–10 days (de Villiers et al., 2010; Di Pierro et al., 2011) and in conjunction with the CloudSat satellite to study the optical properties of mixed-phase and ice clouds and haze (Gayet et al., 2009; Grenier et al., 2009). Devasthale et al. (2011) present a 4 yr CALIPSO-based study of the spatial distribution of Arctic aerosols. They find that the largest fraction of the detected aerosol layers occurs below 1 km and maximizes in winter (65 %), due to the development of strong surface-based temperature inversions, whereas in spring and summer a relatively larger fraction of aerosol layers is detected in the free troposphere. The occurrence of smoke aerosol, associated with biomass burning, reaches an annual maximum in the summer (13 % of total aerosol layers) and is below 5 % in all other seasons.

In this study, we examine the ability of CALIOP to provide information on the horizontal and vertical distribution of Arctic aerosols for 2006–2012. Our study however differs from that of Devasthale et al. (2011) in that we provide an analysis of the seasonal evolution of aerosol extinction. We account for the different performance of the CALIOP instrument when it operates under daytime and nighttime conditions. Furthermore we compare CALIOP retrievals to both ground-based and aircraft-based measurements to evaluate the robustness of CALIOP measurements over the Arctic. In Sect. 2 we present a description of the CALIOP dataset. Section 3 documents a detailed comparison of CALIOP retrievals against surface and aircraft in situ measurements of aerosol extinction over the Arctic as well as against ground-based lidar retrievals of aerosol backscatter. This is followed by a discussion of the horizontal, vertical and temporal variations of Arctic aerosol extinction in 2006–2012 (Sect. 4). Finally, Sect. 5 presents our conclusions.

2 Space-borne CALIOP lidar

CALIOP measures the attenuated backscatter intensity at 532 nm and 1064 nm. The 532 nm channel is polarization-sensitive, allowing for the measurement of the two orthogonally polarized components of the signal. From the measured signal, which after geolocation and calibration is denominated level 1, a series of nested algorithms find atmospheric features at increasing horizontal averaging (Winker et al., 2009; Young and Vaughan, 2009). These features are

then classified as clouds or aerosols, and their subtype (clean continental, clean marine, dust, polluted continental, polluted dust and smoke) is determined. Liu et al. (2009) describe the cloud–aerosol separation algorithm and assess its performance. Omar et al. (2009) describe the aerosol type classification algorithm. The inversion to obtain the AOD at both wavelengths is then initiated by assigning an extinction-to-backscatter ratio (called lidar ratio) as a function of the aerosol type. The resulting data product is called level 2.

The CALIOP 532 nm version 3.01 calibration has been validated against aircraft measurements by the NASA Langley airborne high spectral resolution lidar (AHSRL) instrument for a wide seasonal and latitude range covering diverse aerosol and cloud conditions (Rogers et al., 2011). CALIOP's attenuated backscatter shows a very small negative bias relative to AHSRL both at nighttime ($-2.7\,\% \pm 2.1\,\%$) and daytime ($-2.9\,\% \pm 3.9\,\%$) but lies within the uncertainties of AHSRL (Rogers et al., 2011). No seasonal, latitudinal or vertical dependencies were found. Over the Arctic, CALIOP attenuated backscatter values were within 10 % of AHSRL measurements for all validation flights.

An important aspect of CALIOP's performance is its sensitivity to illumination conditions. Daytime retrievals are less accurate than nighttime retrievals because they are affected by the noise from scattering of solar radiation in the field of view of the detector (Winker et al., 2009; Rogers et al., 2011). Daytime retrievals thus have a higher backscatter sensitivity threshold ($\sim 0.5\,\mathrm{Mm^{-1}\,sr^{-1}}$ at sea level) compared to nighttime retrievals ($\sim 0.4\,\mathrm{Mm^{-1}\,sr^{-1}}$). Both thresholds decrease exponentially with altitude (Winker et al., 2009, 2013), such that at 8 km altitude their values are $\sim 0.3\,\mathrm{Mm^{-1}\,sr^{-1}}$ and $\sim 0.2\,\mathrm{Mm^{-1}\,sr^{-1}}$ for daytime and nighttime, respectively. Over the Arctic, especially in the middle and upper troposphere, thin aerosol layers often have backscatter values below these thresholds and can thus go undetected by CALIOP. The difference in sensitivity between day and night leads to complications in the interpretation of spring and summer retrievals over the Arctic when only daytime measurements are available from CALIOP. We address this issue in more detail in Sect. 2.3.

In this study, we use version 3.01 level-2 Cloud and Aerosol Layer data at 5 km horizontal resolution between June 2006 and October 2011. Between November 2011 and May 2012, we use version 3.02. No differences in the inversion algorithm were introduced between the two versions. The CALIPSO orbit inclination of 98.2° provides coverage up to 81.8° N latitude. We grid the daily CALIOP level-2 5 km orbit segments onto a 2° latitude by 2.5° longitude horizontal grid for all latitudes poleward of 59° N, with 200 m resolution in the vertical. For each grid box we calculate the aerosol detection frequency (f), which is the ratio of the number of detected layers over the sum of detected layers and clear air. We also extract the backscatter (β) and extinction (b_{ext}) of the detected layers along with their standard deviation. The "gridded extinction", $\overline{b_{\mathrm{ext}}}$, is then defined as the product between the aerosol detection frequency and the extinction of the detected layers, $f \times b_{\mathrm{ext}}$. The "gridded backscatter", $\overline{\beta}$, is defined similarly as $f \times \beta$. We will refer to these two gridded products as the standard extinction and backscatter.

This gridding approach assumes that all layers that are undetected by CALIOP (clear air) have an extinction of $0\,\mathrm{Mm^{-1}}$. The same approach was used by Winker et al. (2013), who notes that this assumption likely leads to an underestimate of the true extinction as undetected aerosol layers could have an extinction between $0\,\mathrm{Mm^{-1}}$ and the CALIOP detection threshold. This approach thus yields a lower bound estimate of the true extinction. An alternative approach would be to assign to clear-air extinction values equal to the CALIOP detection threshold. This would result in an upper bound estimate. We will examine the impact of these assumptions in Sect. 3.

2.1 CALIOP data selection

We screen the data by selecting only aerosol retrievals with an absolute value of the cloud aerosol distinction (CAD) confidence function greater than 50. CAD values measure the confidence in the algorithm classification of an atmospheric feature as either a cloud or an aerosol (Liu et al., 2009). CAD values vary between -100 for a feature that is unambiguously classified as an aerosol layer to $+100$ for a feature that is unambiguously classified as a cloud layer. We found that using larger CAD threshold values (up to $|\mathrm{CAD}| = 90$) does not affect our results significantly. We apply a further screening by using the quality control (QC) flag, and exclude aerosol retrievals that yield unphysical solutions or where the retrieval algorithm had to adjust the initially selected lidar ratio. In these cases the retrieved extinction is not accurate, and the uncertainty cannot be estimated (Winker et al., 2009; Young and Vaughan, 2009). We also exclude aerosol layers with unrealistically high extinction values ($> 500\,\mathrm{Mm^{-1}}$).

In version 3.01 an underestimate of aerosol extinction at low levels present in data version 2 was corrected by extending the aerosol layer base to 90 m above the surface. However, this correction leads to unrealistically low extinction at the surface (Koffi et al., 2012). To correct this artifact we apply the same correction as in Koffi et al. (2012) by further extending the lowest aerosol layer to the surface if the height above the surface is less than 10 % of the layer thickness.

Clouds are generally optically thicker than aerosols and can significantly, if not completely, attenuate the lidar signal and thus reduce CALIOP's ability to detect faint features below them. In our study we consider both cloud-free CALIOP profiles as well as profiles above the highest cloud top detected. In a recent study, Yu et al. (2010) used an alternate cloud-screening method, considering cloud-free profiles and allowing thin cirrus (optical depth <0.1) with cloud base greater than 7 km. Using 1 yr of observations we compared

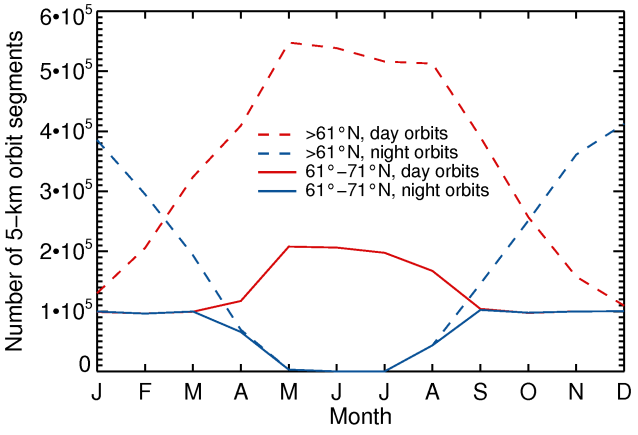

Fig. 1. Number of CALIOP 5 km orbit segments as a function of month for the year 2007. Blue lines indicate nighttime retrievals, whereas red lines are for daytime. Solid lines correspond to the latitude interval 61° −71° N and dashed lines are for the region poleward of 61° N.

results following our approach ("above clouds") to the Yu et al. (2010) approach. We find that the two selection methods yield gridded extinctions that are within 10 % at all altitudes, but our "above clouds" approach allows us to retain three times as many CALIOP layers between 3 and 8 km. In order to increase the number of CALIOP observations, our results will be based on the "above clouds" selection method.

2.2 Diamond dust screening

During the months of December–February, we found that 5 % of the time CALIOP retrieved very high values of aerosol extinctions ($> 300\,\mathrm{Mm}^{-1}$) poleward of 70° N and below 2 km altitude. This distribution is consistent with the reported frequency of occurrence of diamond dust (Intrieri et al., 2004). These anomalously high extinction occurrences could thus be associated with the misclassification of diamond dust as aerosol in the CALIOP retrieval algorithm. The CALIOP feature classification algorithm employs the measured depolarization ratio to help discriminate between clouds and aerosols and is designed to classify diamond dust as "cloud". However, mixtures of aerosols with small quantities of ice crystals are not infrequent (Bourdages et al., 2009) and can exhibit low depolarization ratios but elevated backscatter returns (Hoff, 1988). Under these circumstances the depolarization ratio may be ineffective in helping to correctly identify diamond dust. We eliminate these diamond dust events misclassified as aerosols by removing aerosol layers with extinction values greater than $350\,\mathrm{Mm}^{-1}$ occurring below 2 km between September and May. This results in discarding fewer than 4 % of aerosol layers.

2.3 Combining daytime and nighttime data

Figure 1 shows the seasonal variation in the number of 5 km orbit segments over the Arctic (poleward of 65° N) along the night and day sides of CALIOP's orbit. Daytime orbit segments dominate between March and September, with no nighttime observations at all in May, June and July. If we restrict the orbit segments to the lower Arctic (61–71° N), we find that over a 7-month period (September to March) the number of CALIOP daytime and nighttime orbit segments is the same. We choose this latitude band to compare daytime and nighttime aerosol retrievals for 2006–2012, as shown in Fig. 2.

We separate the months of September through November (SON) and December through March (DJFM) (Fig. 2a, c). For both time periods the backscatter of detected aerosols decreases rapidly with increasing altitude, from 1.5–2 Mm^{-1} near the surface to values $<0.5\,\mathrm{Mm}^{-1}$ above 6 km altitude. The backscatter of detected layers is similar for daytime and nighttime orbits, with daytime backscatter being 10–15 % higher than nighttime. We find much larger differences in the daytime and nighttime aerosol detection frequency (Fig. 2b, d). For nighttime retrievals, the aerosol detection frequency decreases from 20–30 % near the surface to values <1 % above 5 km altitude. The daytime detection frequency is always lower and decreases much more rapidly with altitude, reaching values <1 % above 2 km altitude. This indicates a much-reduced ability of CALIOP to detect aerosols layers over the Arctic during daytime, especially in the free troposphere. We further consider this by examining the ratio between daytime and nighttime detection frequency (shown as a black line in Fig. 2b and d). This ratio decreases from values of 0.4–0.8 near the surface (meaning that during the day 60–20 % fewer aerosol layers are detected than at night) to < 0.1–0.3 above 4 km altitude. This behavior is the result of the rapid decrease of the backscatter with altitude: a higher fraction of the faint aerosol layers at higher altitudes fall below CALIOP's daytime backscatter sensitivity threshold.

In order to exclude the possibility that a diurnal cycle in relative humidity (RH) drives the difference in extinction and aerosol detection frequency between daytime and nighttime retrievals, we compare the daily average RH for descending (daytime) and ascending (nighttime) orbits for the same spatial region and temporal period, using the retrievals from the NASA Atmospheric Infrared Sounder (AIRS) onboard the A-train AQUA satellite for 1 yr of data (2006–2007). The two populations differ in the mean by RH = 3 % (daytime higher). We find that the random variable representing the standardized difference of the two means falls within one standard deviation from zero, indicating that the two RH populations can be considered statistically indistinguishable.

The differences in detection thresholds during day and night affect our ability to reconstruct the full seasonal cycle of aerosols over the Arctic, especially between late spring and early fall, when daytime orbits dominate (Fig. 1). To ad-

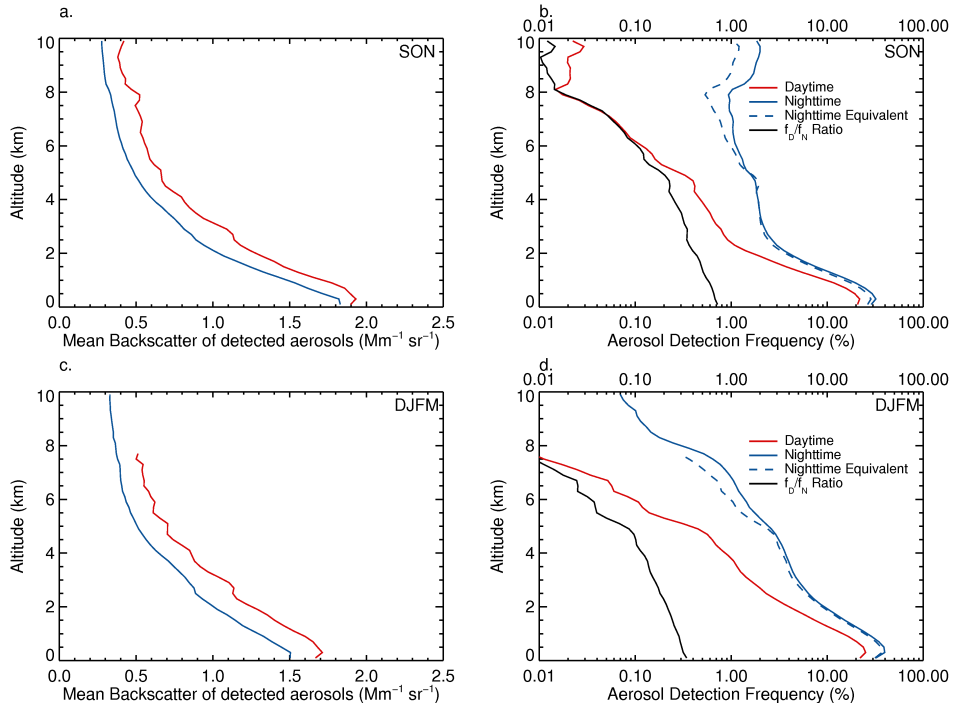

Fig. 2. Backscatter of detected aerosol layers **(a, c)** and vertical profiles of aerosol detection frequency **(b, d)** for 2006–2012 and latitude interval 61°–71° N. Daytime profiles are shown in red; nighttime profiles in blue. The top panels are for the months of September through November (SON), while the bottom panels are for December through March (DJFM). The black line in **(b)** and **(d)** shows the daytime-to-nighttime detection frequency ratio (f_D / f_N). The dashed blue line shows the nighttime-equivalent detection frequency.

dress this issue, we have developed an empirical method that derives a "nighttime-equivalent" gridded extinction; that is, the extinction that would be retrieved if all retrievals took place under nighttime conditions. We consider the CALIOP dataset (2006–2012) in the latitude range 61–71° N for the September–March period. For each grid box within the domain, we calculate the ratio between daytime and nighttime detection frequency ($\frac{f\mathrm{D}}{f\mathrm{N}}$) and the mean backscatter of all detected layers (β). Figure 3 shows the two-dimensional frequency distribution as a function of β and the $\frac{f\mathrm{D}}{f\mathrm{N}}$ ratio. The smallest ratios occur for optically thin aerosols, consistent with Fig. 2, whereas for optically thicker aerosols the daytime detection frequency tends to approach the nighttime detection frequency. The mean ratio for each backscatter bin is indicated by black circles in Fig. 3. Despite considerable scatter in the frequency distribution, the mean ratio falls along a straight line. The linear total least-squares fit to the points is $\frac{f\mathrm{D}}{f\mathrm{N}} = -0.114 + 0.522 \cdot \beta$, with β in Mm^{-1} sr^{-1}. We use this empirical relationship to scale the daytime detection frequency as a function of the mean backscatter of the detected layers by taking the reciprocal of the detection frequency ratio, which we will refer to as our scaling factor, SF:

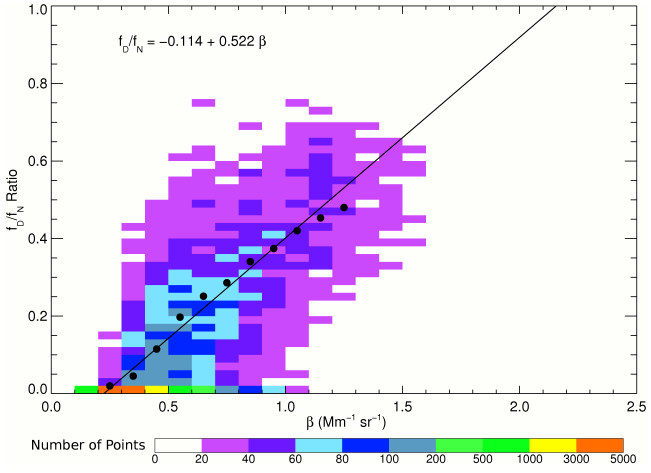

Fig. 3. Scatterplot of the daytime-to-nighttime aerosol detection frequency ratio (f_D / f_N) as a function of the mean backscatter of the detected aerosols, β, for 61°–71° N latitude from September through March, 2006–2012. Colors represent the number 5 km orbit segments in each 2-D bin. Black circles correspond to the average value of (f_D / f_N) for each value of mean backscatter. The straight line is the weighted reduced major axis linear fit to the black circles.

$$\mathrm{SF} = 1 / (-0.114 + 0.522 \cdot \beta). \quad (1)$$

Table 1. Summary of in situ and CALIOP extinctions at Barrow and Alert.

	Station					
	Barrow			Alert		
Years	2006–2011			2006–2008		
Location	71.3° N; 156.6° W			82.5° N; 62.5° W		
Height	8 m			220 m		
Extinctions	Mean $\pm 1\sigma$ (Mm^{-1})	Correlation r	CALIOP Bias[a]	Mean $\pm 1\sigma$ (Mm^{-1})	Correlation r	CALIOP Bias[a]
CALIOP Standard[b]	9.9 ± 11	0.69	−14 %	4.6 ± 5.3	0.75	+15 %
CALIOP Nighttime-Equivalent[b]	11 ± 11	0.68	−2 %	5.0 ± 5.2	0.80	+23 %
CALIOP Upper Bound[c]	23 ± 8.3	0.65	+49 %	19 ± 2.7	0.71	+159 %
In situ	16 ± 9.1	–	–	7.3 ± 6.9	–	–
In situ with CALIOP threshold	11 ± 9.6	–	–	4.0 ± 5.5	–	–

In situ extinction observations are scaled to ambient relative humidity. Three gridded CALIOP extinctions are listed: standard (assuming that clear air has an extinction of $0\,Mm^{-1}$), nighttime equivalent (taking into account the day/night detection threshold and assuming that clear air has an extinction of $0\,Mm^{-1}$) and upper bound (assuming that clear air has an extinction equal to the CALIOP detection threshold).
[a] The CALIOP bias is based on the annual mean values: 100 × (CALIOP-in situ)/in situ.
[b] Correlations and biases are calculated against in situ observations with CALIOP threshold applied.
[c] Correlations and biases are calculated against in situ observations without applying CALIOP threshold.

The nighttime-equivalent gridded extinction, $\overline{b_{\text{ext}}}$, is then calculated by combining the nighttime gridded extinction with the scaled daytime gridded extinction:

$$\overline{b_{\text{ext}}} = (f_{\text{N}} \cdot b_{\text{ext,N}} \cdot N_{\text{N}} + f\text{D} \cdot \text{SF} \cdot b_{\text{ext,D}} \cdot N_{\text{D}}) / (N_{\text{N}} + N_{\text{D}}). \quad (2)$$

where the subscripts N and D indicate nighttime and daytime, b_{ext} is the mean extinction of the detected layers, f is the detection frequency of aerosol layers and N is the number of 5 km orbit segments. The scaling factor is kept in the range 1–50, and the scaled daytime detection frequency $f_{\text{D}} \cdot \text{SF}$ is capped at 100 %. Mean values for SF range from 1.6–2 at 0–2 km to 5.5–6.2 at 4–6 km.

In obtaining the scaling factor (Eq. 1), we use the mean backscatter obtained from both daytime and nighttime retrievals on the x axis of Fig. 3. As shown in Fig. 2, the daytime backscatter is 10–15 % higher than the nighttime backscatter. Using only daytime backscatter in constructing Fig. 3 leads to a much higher scatter and a less statistically robust relationship. The nighttime-equivalent approach assumes that, for daytime retrievals, aerosols layers between the daytime and nighttime detection thresholds have the same extinction as the layers that are detected (Eq. 2). We recognize that this results in an overestimate of the correction (10–15 % during summer and less than 7 % for other seasons). However, this is small compared to the large values of the scaling factors (100–300 %). The nighttime-equivalent extinction also assumes that aerosols undetected at nighttime have zero backscatter and extinction.

The nighttime-equivalent detection frequency ($f_{\text{N}} \cdot N_{\text{N}} + f_{\text{D}} \cdot \text{SF} \cdot N_{\text{D}}) / (N_{\text{N}} + N_{\text{D}})$ is very close to the nighttime detection frequency (f_{N}) (Fig. 2b, d), indicating that the linear fit derived in Fig. 3 is reasonable and produces self-consistent results. In the next section, we compare CALIOP extinction retrievals and our empirical nighttime-equivalent extinctions to ground-based and aircraft observations over the Arctic.

3 Comparisons of CALIOP extinction retrievals with independent measurements

3.1 Surface in situ measurements

We compare the CALIOP extinctions to nephelometer measurements at Barrow (Alaska, USA) and Alert (Nunavut, Canada) (Table 1 and Fig. 4). Ambient air is drawn into the nephelometers via a heated inlet, which desiccates the aerosols by decreasing the relative humidity (RH) to values below 30 %. The cut-off diameter of the inlet nozzle is 10 µm (Delene and Ogren, 2002; Garrett et al., 2011). The sample volume is then illuminated with green light (550 nm); the scattering by aerosol particles is integrated over a broad range of angles (7–170°) to yield the scattering coefficient, b_{scat}. The absorption coefficient (b_{abs}) is also measured by a particle soot absorption photometer at both stations. The extinction coefficient is obtained by adding b_{scat} and b_{abs}. When absorption measurements are not available we assume $b_{\text{ext}} \cong b_{\text{scat}}$. This is a reasonable approximation since b_{abs} is generally less than 5 % of b_{scat} for Arctic aerosols (Delene and Ogren, 2002). Whereas for Barrow the data is already daily averaged, for Alert hourly averages are used, and we require at least eight measurements per day to calculate the daily mean.

When comparing satellite observations with ground measurements, a common problem is the coincidence in space and time between surface measurements and satellite retrievals. This is particularly exacerbated for CALIOP given its narrow footprint. Anderson et al. (2003) demonstrate that at a distance of 160 km spatial correlation between simultaneous measurements has decreased to a value of 0.8, and beyond this distance the correlation rapidly falls. We thus extract CALIOP extinctions in boxes around Alert and Barrow with mean distances from the stations of 170 km and 200 km, respectively. The box size is a compromise between the need

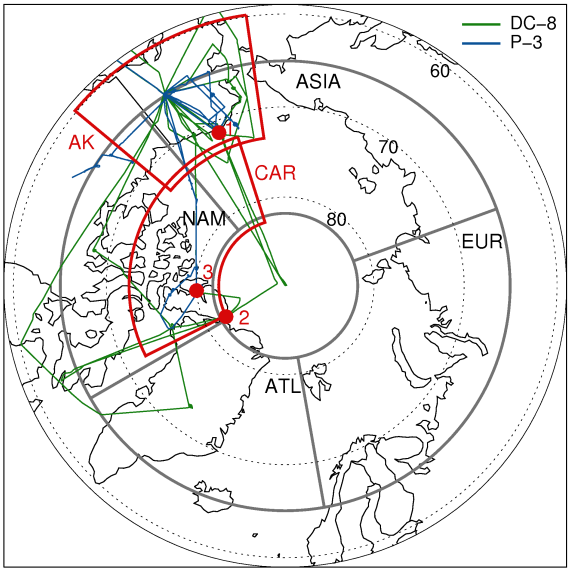

Fig. 4. Arctic map with the location of observations used in this study. Red circles indicate the ground stations: (1) Barrow, (2) Alert and (3) Eureka. The ARCTAS DC-8 (green) and P-3 (blue) flight tracks during April 2008 are also shown. The two regions enclosed by red lines are the domains where CALIOP is compared to ARCTAS measurements: Canadian Arctic (CAR) and Alaska (AK). Grey lines define the four Arctic sectors used in this study: European (EUR), Asian (ASIA), North American (NAM) and Atlantic (ATL).

for a statistically sufficient number of CALIOP points and the ability of the station to effectively represent the surrounding region. The box around Alert is smaller in size because more CALIOP overpasses occur in the vicinity of this high-latitude station relative to the lower latitude of Barrow. These box sizes are also consistent with the temporal resolution (1 day) and the maximum temporal offset between in situ observation and satellite overpasses (∼8 h) assuming a typical horizontal transport velocity of $5\,\mathrm{m\,s^{-1}}$. In order to compare CALIOP and in situ measurements, we require a minimum of ten 5 km CALIOP orbit segments in any given day. We use the CALIOP gridded extinction for the two lowermost vertical levels (0–400 m).

For comparison to CALIOP, we adjust the in situ dry aerosol scattering measurements to ambient RH following Gassó et al. (2000):

$$b_{\mathrm{scat,amb}} = b_{\mathrm{scat,dry}} \left(\frac{100 - \mathrm{RH}}{100 - \mathrm{RH}_0} \right)^{-\gamma} \quad (3)$$

where RH_0 is the relative humidity of the dry samples (30 %) and RH is the ambient relative humidity, which is obtained from AIRS satellite retrievals around the stations. The parameter γ is the hygroscopicity factor and is a function of the aerosol type. Gassó et al. (2000) report average values of 0.23 for dust, 0.57 for polluted marine and 0.69 for a clean marine aerosol. Since aerosols at Barrow are a mixture of sea salt and pollution aerosols (Quinn et al., 2002), we choose $\gamma = 0.57$, corresponding to polluted marine. We use the same γ value at Alert.

For comparison with CALIOP, we also examine the impact of applying CALIOP's nighttime backscatter sensitivity threshold to the ambient in situ observations by setting to zero all measurements below the threshold. The extinction threshold is calculated by multiplying the backscatter threshold by a lidar ratio of 40 sr, which is the mean value of the lidar ratio used by the CALIOP algorithm for both Alert and Barrow. Application of this threshold leads to a 30 % decrease in annual-mean observed extinction at Barrow (from 16 to 11 $\mathrm{Mm^{-1}}$) and a 45 % decrease at Alert (from 7.3 to 4.0 $\mathrm{Mm^{-1}}$) as shown in Table 1.

Figure 5 and Table 1 compares in situ observations at Barrow (2006–2011) and Alert (2006–2008) to CALIOP nighttime-equivalent extinctions. At Barrow, the annual-mean CALIOP nighttime-equivalent extinction ($11 \pm 11\,\mathrm{Mm^{-1}}$) is 30 % lower than in situ observations ($16 \pm 9.1\,\mathrm{Mm^{-1}}$). Applying the CALIOP detection threshold to in situ observations ($11 \pm 9.6\,\mathrm{Mm^{-1}}$) yields much better agreement and reduces the CALIOP bias to −2 %. Similar results are found at Alert, where the nighttime-equivalent CALIOP extinction ($5.0 \pm 5.2\,\mathrm{Mm^{-1}}$) displays a 23 % positive bias compared to in situ observations after application of the CALIOP detection threshold ($4.0 \pm 5.5\,\mathrm{Mm^{-1}}$).

At Barrow, CALIOP captures the seasonal cycle observed by a ground-based nephelometer, with a maximum in extinction in December–February and a minimum in May–August (Fig. 5a and b). The correlation coefficient between the monthly mean in situ and CALIOP nighttime-equivalent extinction is $r = 0.68$. Interannual variability is relatively small. Quinn et al. (2002) found that the light extinction seasonal cycle at Barrow is controlled by sea salt in October–January, associated with influx from the northern Pacific Ocean, and by non-sea-salt sulfate in March–June, caused by the transport of pollution from midlatitude sources. In the summer, efficient wet scavenging and reduced inflow from midlatitudes leads to a minimum. At Alert, CALIOP also reproduces the observed seasonal cycle, with an extinction maximum in November–March and a minimum in June–September. In summer, aerosol extinctions decrease to values that are often well below the detection limit of CALIOP.

We note that the CALIOP extinctions tend to underestimate in situ observations during spring (March–May) by 37 % at Barrow and 63 % at Alert (Fig. 5b and d). This is unlikely to be related to our assumption of a constant $\gamma = 0.57$ in the conversion of in situ extinctions to ambient RH. For example, using $\gamma = 0.35$ during the March–May period, reflecting less hygroscopic biomass burning aerosols, would only slightly reduce the CALIOP underestimate (Barrow: 28 %; Alert: 56 %).

We also examine the impact of not taking into account the night–day difference (SF = 1) and define the "standard extinction" by setting clear-air extinction to $0\,\mathrm{Mm^{-1}}$

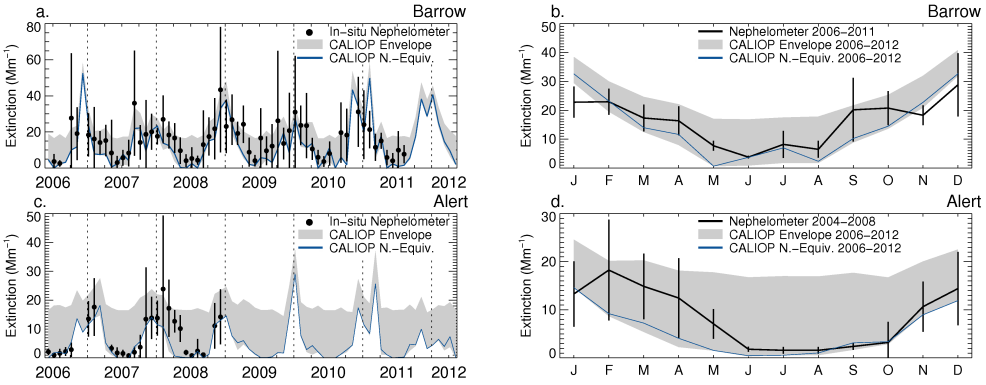

Fig. 5. Comparison between monthly mean CALIOP 532 nm and in situ 550 nm extinctions at Barrow (top row) and Alert (bottom row). Left panels (**a** and **c**): Black full circles indicate the in situ monthly mean extinctions, with vertical bars indicating one standard deviation of the daily observations. The in situ extinctions are scaled to ambient RH. The blue line shows CALIOP nighttime-equivalent mean extinction, with grey shading indicating the envelope of CALIOP retrievals (see text). Right panels (**b** and **d**): CALIOP 2006–2012 climatological mean extinction (blue line: nighttime-equivalent; grey shading: CALIOP envelope) are compared to the in situ seasonal mean extinction (black line). For Barrow the in situ climatological mean extinctions are for year 2006–2011, but for Alert we use years 2004–2008.

(see Table 1 and Fig. 5, lower bound of the grey envelope). We find that there is little difference between the CALIOP standard extinctions (Barrow: $9.9 \pm 11\,\mathrm{Mm}^{-1}$; Alert: $4.6 \pm 5.3\,\mathrm{Mm}^{-1}$) and nighttime-equivalent extinctions (Barrow: $11 \pm 11\,\mathrm{Mm}^{-1}$; Alert: $5.0 \pm 5.2\,\mathrm{Mm}^{-1}$) because the annual mean values are dominated by the winter maxima which occur under nighttime conditions. As we will see in Sects. 3.2 and 3.3, the difference between the two estimates is more pronounced at higher altitudes, where the aerosol layers are less dense.

Our calculated CALIOP nighttime-equivalent extinctions at Barrow and Alert represent a lower bound of the true extinctions, as we assume that when no layer is detected by CALIOP, the extinction is $0\,\mathrm{Mm}^{-1}$. We calculate an upper-bound CALIOP extinction at these stations by setting SF = 1 and the extinction of clear air to a value equal to the appropriate (day or night) CALIOP detection threshold (see Table 1 and Fig. 5, upper bound of the grey envelope). These upper-bound gridded extinctions overestimate the in situ annual-mean extinction by 50 % at Barrow (upper bound: $23\,\mathrm{Mm}^{-1}$; in situ: $16\,\mathrm{Mm}^{-1}$) and 160 % at Alert (upper bound: $19\,\mathrm{Mm}^{-1}$; in situ: $7.3\,\mathrm{Mm}^{-1}$). At Alert the seasonal cycle of the upper bound is weaker compared to in situ observations. In situ observations are much closer to the nighttime equivalent in the summer, showing that the true extinction of the undetected layers is much below the sensitivity threshold.

3.2 ARCTAS aircraft measurements

During the NASA ARCTAS campaign, nephelometers onboard the DC-8 (Anderson et al., 1998) and P-3 aircraft (Anderson and Ogren, 1998) measured aerosol scattering coefficients at 550 nm. Concurrent measurements of the scattering enhancement factor and ambient RH allow for the calculation of the scattering coefficient at ambient RH, as described in Shinozuka et al. (2011). The total extinction at 550 nm is obtained by adding the scattering coefficient at ambient RH to the single-particle soot photometer absorption measurements (Clarke et al., 2004).

In analyzing ARCTAS April 2008 measurements we consider two regions: the Canadian Arctic (CAR: 72.5–82.5° N, 62.3–162.3° W) and Alaska (AK: 59.8–73.3° N, 127.9–171.8° W), as shown in Fig. 4. Thick aerosol plumes (with CO > 200 ppbv or $b_{\mathrm{ext}} > 150\,\mathrm{Mm}^{-1}$) are excluded from the ARCTAS dataset. We calculate the CALIOP mean extinction profiles for these two regions on the days when flights took place (9 DC-8 flights and 7 P-3 flights over AK; 5 DC-8 flights and 2 P-3 flights over CAR). Bian et al. (2013) demonstrated that the ARCTAS measurements along the flight track were representative of regional averages during spring 2008. Figure 6 shows the in situ extinction profiles observed during the April 2008 ARCTAS deployment over the AK region. The largest extinctions are observed near the surface ($20–30\,\mathrm{Mm}^{-1}$) with a secondary maximum at 3–4 km. Over the CAR region, the surface maximum reaches lower values (Fig. 7), but the profile also displays a secondary maximum in the mid-troposphere.

We compare observed in situ extinctions to the CALIOP 80 km sensitivity thresholds (Fig. 6). In order to convert the CALIOP backscatter threshold to extinction, we use a lidar ratio of 60 sr, which is representative of the smoke aerosols prevalent during ARCTAS (Burton et al., 2012). We find that 83 % of the ARCTAS observations in spring are below the CALIOP nighttime sensitivity threshold (AK: 76 %; CAR: 96 %). CALIOP would thus only be able to detect the strongest haze events. Figure 7 displays the in situ mean extinction profiles with the CALIOP 80 km nighttime backscatter sensitivity threshold applied (extinction measurements

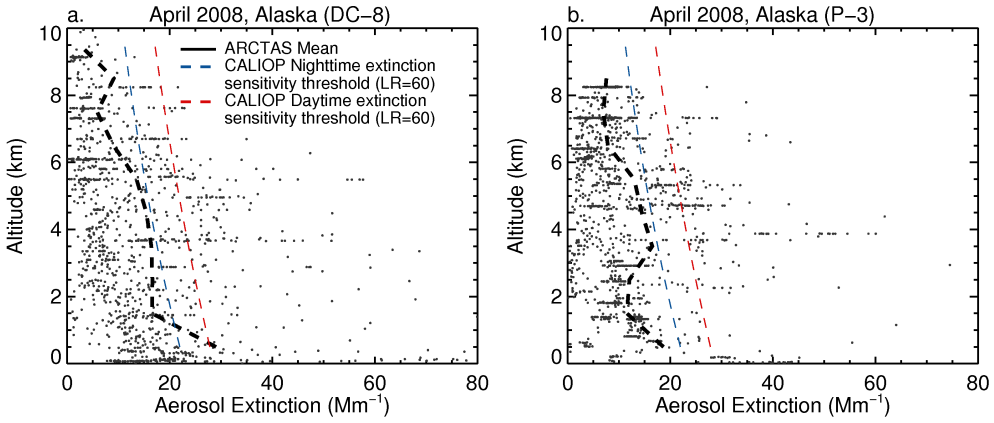

Fig. 6. ARCTAS mean extinction profiles for April 2008 over the AK domain shown in Fig. 4 for the DC-8 **(a)** and P-3 **(b)** aircraft platforms. The ARCTAS 1 min average measurements are shown with grey dots, whereas their altitude-binned mean is shown with a dashed black line. All measurements are corrected to ambient RH. The CALIOP daytime and nighttime extinction detection thresholds are also shown with a red and blue dashed line respectively, assuming a lidar ratio of 60 sr (see text).

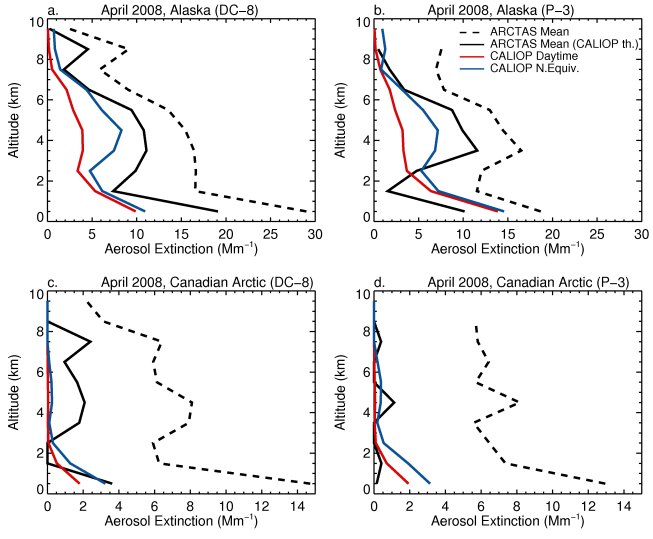

Fig. 7. Comparison between CALIOP and ARCTAS mean extinction profiles for the DC-8 and P-3 flight days over AK **(a, b)** and CAR **(c, d)** in April 2008. In situ aircraft profiles of extinctions are shown with (solid black line) and without (dashed black line) the CALIOP nighttime threshold applied. The red line shows the CALIOP standard (daytime) mean extinction profile, whereas a blue line indicates the nighttime-equivalent mean extinction profile.

corresponding to values of backscatter below this threshold are set to zero). The resulting observed extinction profile is significantly reduced, with column-integrated AOD decreasing by 45 % over Alaska (from 0.12 to 0.065) and by 90 % over the Canadian Arctic (from 0.065 to 0.007). The retrieved daytime CALIOP extinction profiles during ARCTAS (red lines) have very low extinction values, typically below 5 Mm^{-1} over Alaska and below 2 Mm^{-1} over the Canadian Arctic. After we apply our scaling factor (Sect. 2.3), the nighttime-equivalent CALIOP profiles (blue lines) exhibit extinction values up to 7–8 Mm^{-1}. Over Alaska, the CALIOP nighttime-equivalent mean extinction profile has a shape that is similar to the in situ observations with threshold applied: high values near the surface and a secondary maximum at 3–6 km (Fig. 7a, b). The CALIOP nighttime-equivalent is 20 % lower than in situ measurements, with a column AOD of 0.05 (in situ observations after threshold: 0.065). Over the Canadian Arctic (Fig. 7c, d) aircraft observations were much sparser. In addition, the measured extinction was lower than over AK, causing even fewer points to survive the application of CALIOP's threshold. Despite these limitations, CALIOP reproduces to some extent the shape of the profiles. We note that for the summer ARCTAS deployment, observed extinctions are so low that they are below CALIOP's threshold all the time, and are thus not shown here.

3.3 High spectral resolution lidar at Eureka, Canada

We compare CALIOP backscatter retrievals with the backscatter measured by the high spectral resolution lidar (HSRL) at Eureka, Nunavut, Canada (80.0° N, 86.0° W, 10 m a.m.s.l.). The University of Wisconsin has operated this lidar since 2006 (Eloranta et al., 2006). A millimeter cloud radar also operates at the site, and we use its backscatter return to mask out clouds and precipitation. The lidar is aligned 4° off the zenith to avoid reflection from horizontally oriented ice crystals (HOI). In computing the HSRL mean profile we consider only clear-sky profiles for the January to April period of 2007–2009. We exclude the months of April 2007 and January–February 2008 because of data quality issues related to instrumentation failures. To discriminate aerosols from other atmospheric scatterers, we apply a linear depolarization threshold of 10 %. This value is con-

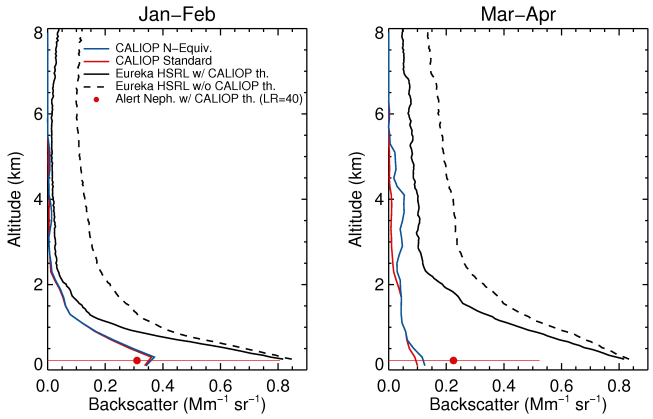

Fig. 8. Vertical profiles of 180° backscatter observed by the ground-based HSRL at Eureka, Nunavut, Canada (80.0° N, 86.0° W) for January–February (left panel) and March–April (right panel) 2007–2009. The HSRL backscatter profiles with (solid black line) and without (dashed black line) the CALIOP nighttime threshold applied are compared to the CALIOP nighttime-equivalent backscatter (blue line) and standard backscatter (red line). The median aerosol backscatter measured at the nearby station of Alert is obtained by dividing the measured extinction by a lidar ratio of 40 sr, and is shown with and without the CALIOP threshold.

sistent with previous measurements of aerosol depolarization ratio at Eureka (Ishii et al., 2001). While aerosol extinctions are also retrieved by the Eureka HSRL, the values are very noisy because of the very small field of view of the receiver. We thus choose to compare the HSRL backscatter to the CALIOP backscatter, averaged within $\pm 1°$ latitude and $\pm 5°$ longitude centered at Eureka, resulting in an average distance with the satellite footprint of less than 110 km.

Figure 8 shows CALIOP and HSRL vertical profiles of aerosol 180° backscatter for January–February (JF) and March–April (MA). In JF, HSRL measurements show a maximum of 0.8 Mm^{-1} sr^{-1} below 1 km, where 40 % of the column-integrated backscatter resides (dashed black line, left panel). In MA the column-integrated backscatter is 40 % higher than in JF. The bulk of this enhancement in backscatter (> 85 %) occurs above 1 km. This seasonal change in the aerosol vertical distribution is indicative of enhanced aerosol influx in the free troposphere.

Applying CALIOP's nighttime sensitivity threshold to the HSRL measurements leads to a mean 10–15 % decrease in backscatter below 1 km and a larger (50–75 %) decrease above 1 km (black solid line). The nighttime-equivalent CALIOP backscatter reproduces the shape of the profiles but is systematically too low by a factor of 2–8 below 5 km. We find that the nighttime-equivalent backscatter qualitatively reproduces the MA mid-tropospheric backscatter enhancement (blue line, right panel), whereas the standard backscatter shows values similar to those observed in JF (red line, right panel). The vertical partitioning of aerosol backscatter is consistent between the two sensors: CALIOP observes 73 % of the vertically integrated backscatter below 1 km in winter (HSRL with sensitivity threshold: 70 %), whereas this fraction decreases to 35 % in spring (HSRL with sensitivity threshold: 46 %).

The CALIOP systematic underestimate could be due to the fact that too many aerosol layers above Eureka have extinctions below the CALIOP detection threshold, as was found in our ARCTAS comparison over the Canadian Arctic (Fig. 7c, d). There could also be potential issues with our retrieval of aerosol backscatter from the HSRL measurements. When we compare the HSRL backscatter to ARCTAS observations in April 2008 above Eureka by assuming a lidar ratio of 60 sr for the in situ measurements, we find that HSRL measurements are a factor of 2 higher than in situ measurements, at all altitudes (not shown). Furthermore, the HSRL backscatter values at the surface are a factor of 2 higher than the ambient backscatter measured at the nearby station of Alert for 2007–2008 (Fig. 8). Though the reason of this overestimate is not clear, we hypothesize that the presence of ice crystals mixed with aerosols might artificially elevate the backscatter retrieved by HSRL.

In summary, our comparison of CALIOP retrievals with independent measurements of aerosol extinction demonstrates that when we take into account the CALIOP sensitivity threshold, the retrieved nighttime-equivalent extinction captures in situ observations to within 25 % in most cases. At the surface, CALIOP reproduces the seasonality of Arctic aerosols as observed at Barrow and Alert. In the free troposphere, CALIOP reproduces the vertical distribution of aerosol layers and their seasonal variations as illustrated by our comparisons to ARCTAS aircraft profiles and HSRL profiles above Eureka. As a result of this sensitivity threshold and the low extinctions of aerosols over the Arctic, only a fraction of the column AOD can be retrieved by CALIOP over the Arctic (e.g., ∼30 % for AK and ∼15 % for CAR in spring; see Sect. 3.2). Exactly how much depends on the column aerosol loading and the vertical distribution of extinction.

4 Results

4.1 Pan-Arctic surface extinction maximum in winter

Figure 9 shows the mean seasonal cycle of CALIOP nighttime-equivalent extinction in the lower (0–2 km), middle (2–5 km) and upper troposphere (5–8 km) over the Arctic for 2006–2012. The Arctic is divided into Low Arctic (59–69° N) and High Arctic (69–82° N). We consider four sectors: European (EUR, 10–110° E), Asian (ASIA, 110° E–140° W), North American (NAM, 140–60° W) and Atlantic (ATL, 60° W–10° E) (see Fig. 4). These sectors are intended to capture the typical transport pathways for short-lived pollutants (5–8 days) following the Lagrangian trajectory studies of Eckhart et al. (2003) and Stohl et al. (2002).

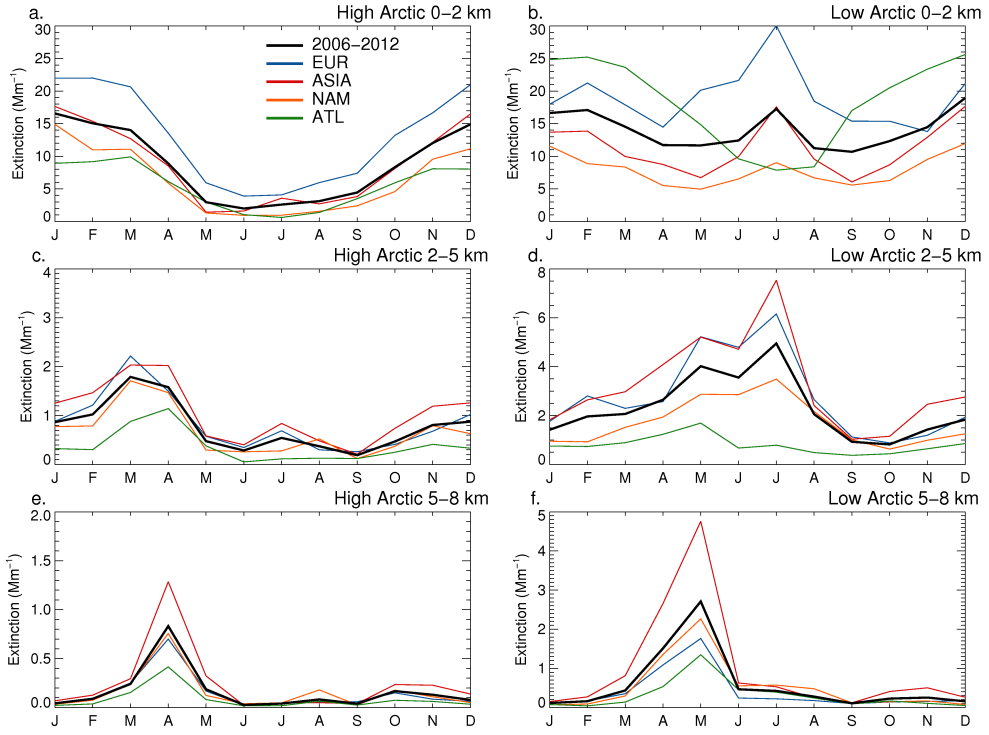

Fig. 9. Seasonal cycle of monthly CALIOP aerosol nighttime-equivalent extinction at 0–2 km (top panels), 2–5 km (middle panels) and 5–8 km (bottom panels) averaged over 2006–2012. Left panels **(a, c, e)** are for the High Arctic (59°–69° N); panels on the right **(b, d, f)** are for the Low Arctic (69°–82° N). The black line corresponds to the mean extinction for the entire High and Low Arctic regions, while colored lines are for the individual Arctic sectors defined in Fig. 4.

In the High Arctic at 0–2 km (Fig. 9a), CALIOP extinctions vary from a minimum of 2 Mm^{-1} to a maximum of 16 Mm^{-1} with an annual mean of 9 Mm^{-1}. The seasonal cycle is the same as at Barrow and Alert with a December–March maximum, followed by a sharp decline and a summer minimum, in agreement with the well-known seasonality of Arctic haze. All four sectors display the same seasonal cycle. The largest extinctions are observed in the European sector during the winter–spring period, consistent with early studies identifying the European/Russian Arctic as the most polluted Arctic sector because of its proximity to western Eurasian sources (Rahn and Lowenthall, 1984; Raatz and Shaw, 1984; Barrie et al., 1989). This finding is also consistent with the recent modeling intercomparison study of Shindell et al. (2008), who found that all atmospheric chemical transport models point to western Eurasia as the largest source region of aerosols and SO_2 at low altitude. CALIOP observations show that the Asian sector displays slightly lower values relative to the European sector, followed by the North American sector. The Atlantic sector is the cleanest, with wintertime extinction values nearly a factor of 2 lower than over the European sector.

The Low Arctic at 0–2 km (Fig. 9b) displays higher CALIOP extinctions (annual mean: 14 ± 3 Mm^{-1}) than the High Arctic. When extinctions are averaged over the entire Low Arctic, there is no clear seasonal cycle. This lack of seasonality comes from the out-of-phase seasonal cycle in the Atlantic sector compared to the other sectors. In the European, Asian and North American sectors there are two maxima: one in December–January and another in July. The summer peak is consistent with measurements of particle number and volume concentration in the planetary boundary layer at the Zotino Tall Tower Facility (ZOTTO) in the Siberian Low Arctic (60.8° N, 89.35° E), which show a June–July maximum in median particle number concentration (June–July: 900 cm^{-3}; November–February: 520 cm^{-3}) and comparable volume concentrations between summer and winter (Heintzenberg et al., 2011). In the Atlantic sector, the seasonality is reversed with a summer minimum and a December–March maximum, corresponding to elevated sea salt aerosol concentrations generated by high winds during winter (see Sect. 4.2).

Figure 10 shows the seasonal mean (2006–2012) horizontal distribution of CALIOP extinction for different altitude ranges. The main feature in the lower troposphere is the large-scale winter (DJF) maximum in extinction (25–40 Mm^{-1}) extending throughout northern Russia. This enhancement is associated with low-level transport of pollution aerosols induced by the meridional circulation along the Siberian anticyclone (Barrie, 1986). An enhancement

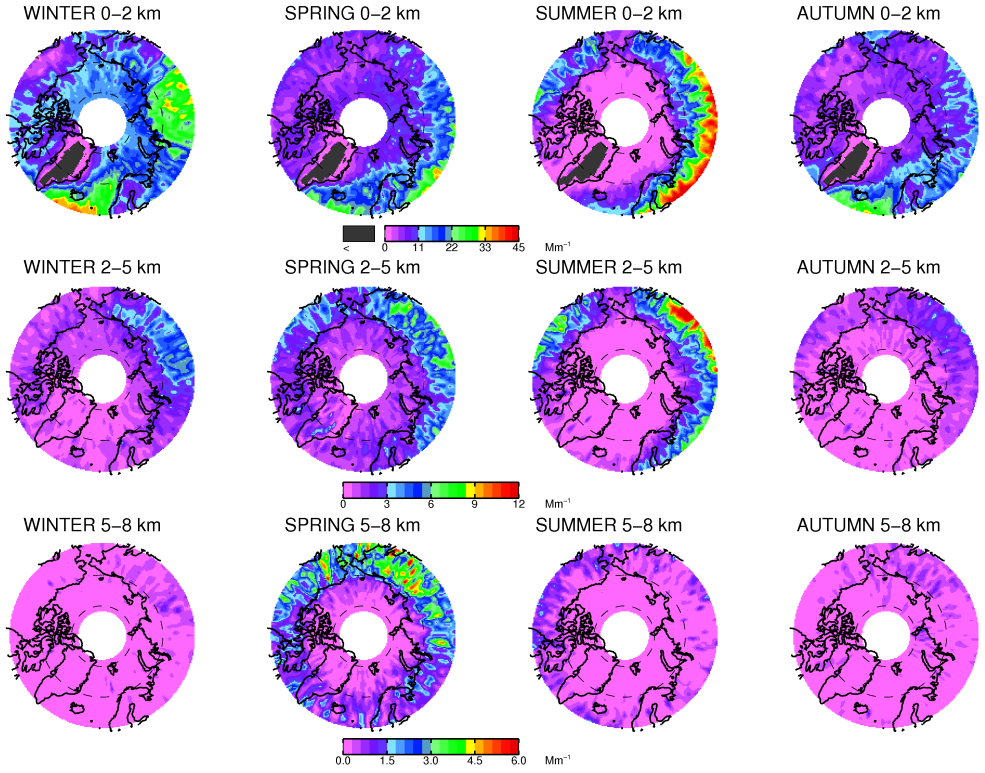

Fig. 10. Spatial distribution of the 2006–2012 seasonal mean CALIOP nighttime-equivalent extinction. Maps are shown at 0–2 km (top panels), 2–5 km (middle panels) and 5–8 km (bottom panels) for winter (DJF), spring (MAM), summer (JJA) and autumn (SON). Note that the color scale saturation values are lowered at higher altitudes. Dashed lines mark the 70° N and 80° N latitude circles.

in extinction is also seen over the central Russian Arctic (5–7 Mm^{-1}) at 2–5 km, which could indicate that a fraction of Eurasian pollution is lifted into the free troposphere by cyclones moving along the western periphery of the Siberian anticyclone (Raatz and Shaw, 1994). Another winter surface maximum is located over the Norwegian Sea and is due to sea salt aerosols produced by the strong wind speeds (Fig. 10). During spring at 0–2 km, extinction values decrease across the entire Arctic, reaching 5–15 Mm^{-1} in the High Arctic.

Figure 11 shows the mean nighttime-equivalent extinction vertical profiles by sector and season for the Arctic poleward of 65° N. Extinction peaks in the lowest 0.5 km in all sectors and seasons but is highest in winter, with mean values of 40 Mm^{-1} for the European sector, and 30 Mm^{-1} for the Asian and North American sectors. Because of the strong stratification of the lower atmosphere in winter and late autumn, extinction drops rapidly with altitude in these seasons. In both winter and autumn, two thirds of the column AOD is found below 1 km.

4.2 Summertime extinction maximum in the Low Arctic due to biomass burning

As noted in Sect. 4.1, CALIOP observes high aerosol extinctions in July in the lower troposphere over the Low Arctic. This July peak is associated with the summertime maximum in forest fire emissions in the boreal regions of Asia and North America (van der Werf et al., 2006) as well as with a maximum in fire intensity (Giglio et al., 2006; Ichoku et al., 2008). Indeed, we find that the CALIOP classification algorithm identifies most of these aerosols layers as "smoke" (not shown).

The summer surface peak in the Low Arctic appears to extend to the middle troposphere (Figs. 9d and 10), indicating efficient vertical mixing of boreal forest fire emissions, and a variety of smoke injection heights. This is also reflected by the shape of extinction profiles in summer, which display a convex shape in all land sectors (Fig. 11). At 0–2 km in July, CALIOP extinctions over the European sector exceed the extinctions in the Asian sector (Fig. 9b). This is reversed at 2–5 km altitude, where we find larger extinction enhancements in the Asian sector compared to the European sector (Figs. 9d, and 10). Retrievals of smoke plume height from space by the Multi-angle Imaging SpectroRadiometer (MISR) over North America show that plumes originating from the burning of boreal forests and shrubland are generally thicker, longer and more elevated than those found over regions characterized by temperate forests (Val Martin et al., 2010). In the Asian and North American sectors, significant burning takes place within the Arctic, and involves the burn-

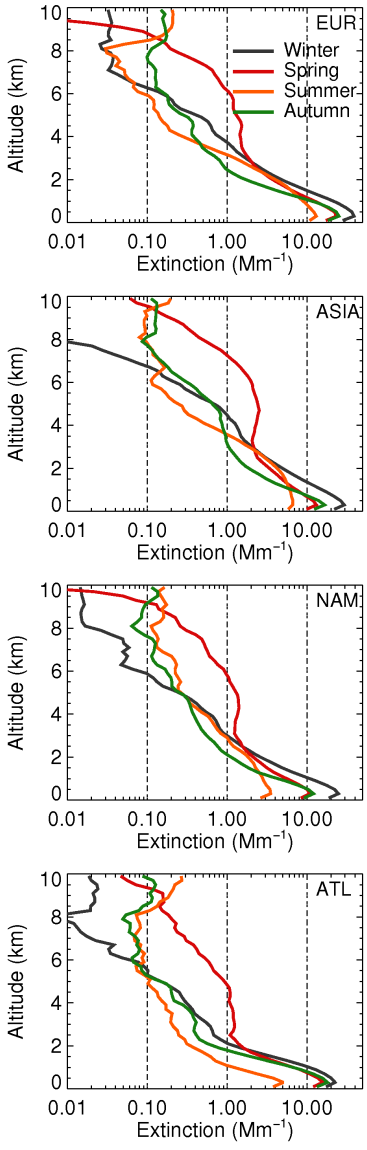

Fig. 11. Mean seasonal vertical profiles of CALIOP nighttime-equivalent extinction for the four Arctic sectors poleward of 65° N (from top to bottom): European, Asian, North American, Atlantic.

ing of boreal forests. In the European sector on the other hand, emissions maximize at lower latitudes (45–60° N) and altitudes, where the dominant biome consists of temperate forests and grassland, and is characterized by fuel loads that are a factor 10–20 lower than those found in the boreal regions (Van der Werf et al., 2006). This contrast in vegetation burned and burning heights could thus explain the different vertical distribution of aerosols in the Low Arctic for different sectors.

4.3 Summertime extinction minimum over the High Arctic: efficient scavenging and slow transport

During summer over the High Arctic, CALIOP extinctions display the lowest aerosol loading (Fig. 9a, c, e). This occurs at all altitudes and for all sectors, as also illustrated in Fig. 11. However, in the Low Arctic, extinction reaches an annual maximum during the summer (Sect. 4.2; Fig. 9b, d). This leads to a strong meridional gradient in aerosol extinction between 60° N and 70° N (Fig. 10).

These very low summertime extinctions over the High Arctic could be associated with efficient wet scavenging that takes place during transport from lower to higher Arctic latitudes. Indeed, the modeling study of Browse et al. (2012) found that summertime stratocumulus drizzle causes a factor 10 decrease in sulfate concentrations at the surface between 60° N and 70° N. Matsui et al. (2012) examined the transport efficiency to the Arctic of BC relative to CO, contrasting spring and summer. They found a factor of 17–20 decrease in the BC transport efficiency between spring and summer, which was due to higher precipitation over the latitudes 45–70° N during summer. In addition to efficient wet removal, the poleward withdrawal of the polar front is also likely to play a role in preventing transport to the High Arctic in summer since the Arctic landmasses constitute a heat source rather than a heat sink (Stohl, 2006). Furthermore, the combination of low aerosol burden and CALIOP's high daytime detection threshold leads to very few aerosol layers being detected in the summer, and might thus further exacerbate the CALIOP aerosol extinction gradient between Low and High Arctic.

4.4 Springtime aerosol extinction maximum in the middle and upper troposphere

In the High Arctic middle troposphere (2–5 km), the CALIOP extinction maximum occurs in March (0.9–2.3 Mm^{-1}), with values a factor 2–3 higher than the annual average (Fig. 9c). At higher altitudes (5–8 km), the peak occurs in April, reaching values of 0.4–1.3 Mm^{-1} (Fig. 9e). We thus see a progressive shift of the extinction maximum with altitude, from January at 0–2 km, to March at 2–5 km, to April at 5–8 km. The springtime middle and upper tropospheric enhancement is apparent in the extinction profiles as well (Fig. 11).

This Arctic spring maximum in the middle and upper troposphere is consistent with meridional transport of pollution from midlatitudes along stable isentropes (Stohl, 2006; Klonecki et al., 2003). Late winter to early spring marks a maximum in cyclonic activity (Klein, 1958; Chen et al., 1991). Cyclones ventilate the planetary boundary layer and inject pollutants into the free troposphere, where they can be rapidly transported over large distances. Once in the free troposphere, a blocking pattern represents a favorable configuration for rapid isentropic poleward transport (Iversen and

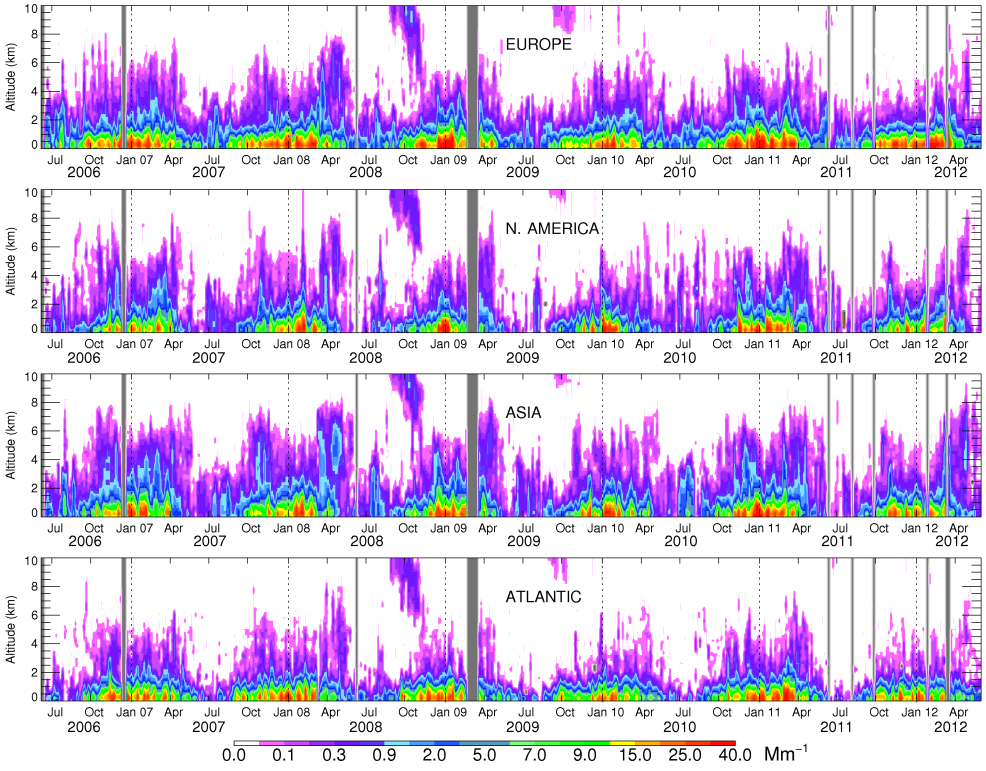

Fig. 12. Timeseries of 5-day-mean nighttime-equivalent CALIOP extinction as a function of altitude for the four Arctic sectors poleward of 65° N. Grey vertical bars indicate CALIOP data gaps.

Joranger, 1985; Di Pierro et al., 2011). The January to March period exhibits the highest frequency of blocking patterns in the Northern Hemisphere (Lejenas and Økland, 1983).

We find high springtime extinctions over most of the Russian and Alaskan Arctic at 2–5 km (Fig. 10). This is consistent with outflow from East Asia. In a previous study using CALIOP observations and a chemical transport model, we examined several Asian long-range transport events reaching the Arctic 3–4 days after export from the boundary layer (Di Pierro et al., 2011). Transport occurred at 3–6 km following a strongly southerly pathway over eastern Siberia and Alaska. Spring is also the season when the occurrence frequency of dust storms is maximum in East Asia (Shao and Dong, 2006). In particular, dust lifted from the Taklimakan Desert follows a northwestward route and is injected at altitudes above 5 km (Sun et al., 2001; Yumimoto et al., 2009). Asian dust could thus potentially reach the Arctic upper troposphere during spring. Indeed, we find that the upper tropospheric April–May CALIOP extinction maximum is particularly strong in the Asian sector (Figs. 9 and 10).

Our results are consistent with observations obtained during the TOPSE aircraft campaign, showing increasing fine-particle sulfate mixing ratios with altitude as the season progressed from February to May over the North American sector (50° N–86° N) (Scheuer et al., 2003). Similarly, Browell et al. (2003) found a 5-fold increase in aerosol number concentration at 4–6 km between February and May during TOPSE. The late spring maximum was also reported by Treffeisen et al. (2006) based on the SAGE satellite retrievals. They attributed it to increased transport from the midlatitudes at this time of year.

4.5 Interannual variability

Among the factors that affect aerosol mass concentration variability on interannual timescales, transport and emissions have been found to play the greatest role and account for 75 % of the observed variability at the surface in the High Canadian Arctic (Gong et al., 2010). Biomass burning emissions display a strong interannual variability, especially in boreal environments (van der Werf et al., 2006). Episodic volcanic eruptions at high latitudes can also contribute to the variability in aerosol loading. Changes in meteorology can affect the efficiency of transport to the Arctic from midlatitudes, but also the scavenging efficiency en route.

Figure 12 shows a time series (5-day mean) of CALIOP extinction as a function of altitude for the four Arctic sectors poleward of 65° N, while Fig. 13 shows the monthly variation in CALIOP extinctions over the High and Low Arctic for the six individual years in our record. There appears to be relatively little interannual variability near the surface, with higher variability in the middle and upper troposphere.

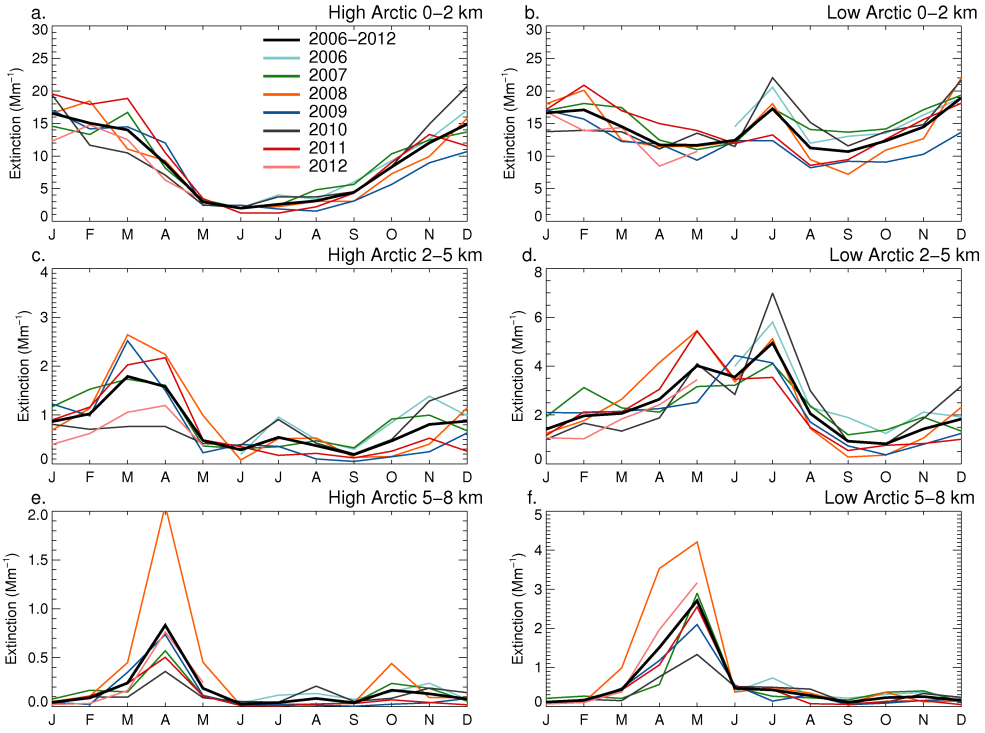

Fig. 13. Same as Fig. 9, but colored lines are for CALIOP nighttime-equivalent extinction for individual years between 2006 and 2012. The black lines correspond to the 6-year average (2006–2012) seasonal cycle of extinction.

In the middle and upper troposphere, spring of 2008 stands out with much larger CALIOP extinctions relative to the multiyear mean. These anomalously high aerosol extinctions were caused by smoke produced during wild and agricultural fires in Russia and Kazakhstan (e.g., Warneke et al., 2009; Fuelberg et al., 2010). July 2010 displays some of the largest summertime extinctions observed by CALIOP (Fig. 13). The enhancements took place over the European and Asian Arctic (Fig. 12), and are consistent with the wildfires that occurred throughout western Russia during the 2010 heat wave. Witte et al. (2011) reported that Moderate Resolution Imaging Spectroradiometer (MODIS) AOD and fire counts over that region during July and August 2010 were a factor of ∼7–8 larger with respect to their 2002–2009 average.

Figures 12 and 13b illustrate the influence of the August 2008 Kasatochi volcanic eruption in the central Aleutian Islands, Alaska. The plume of the Kasatochi eruption reached the lower stratosphere, with smaller plumes reaching up to 18–20 km (Martinsson et al., 2009), followed by mixing subsidence. As can be clearly seen in Fig. 12, the Kasatochi sulfate aerosol plume appears in the Arctic lower stratosphere/upper troposphere in August 2008 and then slowly descends down to 6–7 km altitude, with an extinction maximum occurring at 5–8 km in the High Arctic in October 2008 (Fig. 13e). Figure 12 also exhibits a small aerosol extinction enhancement in September–October 2009 at 8–10 km, which we link to subsidence from the lower stratosphere following the June 2009 Sarychev volcano eruption in the Kuril Islands, Russia (Kravitz et al., 2011).

Particularly low extinctions are observed by CALIOP in November 2009–May 2010 in the High Arctic throughout the troposphere (Fig. 13, left column). This was followed by a period with higher extinctions in November 2010–May 2011. Variations in atmospheric circulation seem to have controlled these changes. During the first period, the Arctic Oscillation (AO) and the North Atlantic Oscillation (NAO) reached an unusually strong minimum in the winter of 2009–2010 (Cohen et al., 2010; Seager et al., 2010). Both indices describe a redistribution of atmospheric mass between the Arctic and the subtropics, with the positive phases of AO/NAO associated with lower than usual sea level pressure over the Arctic and higher sea level pressure over the North Atlantic. These very strong negative values were maintained for most of 2010, and then starting in late 2010 both indices increased, reaching positive phases of AO and NAO in spring 2011 (http://www.cpc.ncep.noaa.gov/). The changes in these indices track changes in CALIOP extinctions, with reduced transport with low aerosol extinctions during negative phases of the NAO/AO and enhanced transport with high aerosol extinctions during positive phases of the NAO/AO. This is consistent with the findings of Eckhart et al. (2003) and Duncan and Bey (2004), who showed that positive phases of the North Atlantic Oscillation (NAO) and Arctic Oscillation (AO) promote enhanced pollution transport to the Arctic

from Europe and North America, particularly in winter and spring.

5 Conclusions

We present a 6-year altitude-resolved distribution of aerosol extinction over the Arctic, retrieved from the CALIOP lidar onboard the CALIPSO satellite between June 2006 and May 2012. As the lower CALIOP detection sensitivity during daytime significantly impacts the retrieval of optically thin Arctic aerosol layers, we developed an empirical methodology to take into account this sensitivity, allowing for us to reconstruct the full seasonal cycle of Arctic aerosols through the definition of a nighttime-equivalent extinction.

We compared the CALIOP nighttime-equivalent extinction to in situ measurements of aerosol extinction at Barrow (Alaska) and Alert (Canada). CALIOP was able to reproduce the observed magnitude of the extinction to within 25 % and captured the seasonal variation at both sites. The nighttime-equivalent extinction was also compared to extinction profiles measured during the NASA ARCTAS aircraft campaign in April 2008. Roughly 80 % of the measurements fell below CALIOP sensitivity threshold, more so in the Canadian High Arctic (96 %) than over Alaska (76 %). When the CALIOP sensitivity threshold was applied to in situ measurements, the observed column AOD was reduced by 50 % and we found that CALIOP nighttime-equivalent extinction reproduced the altitude of the observed extinction maxima, while capturing 80 % of the column AOD.

Additionally, we used the HSRL at Eureka (80° N, 86° W) to validate the seasonal evolution of aerosol 180° backscatter profiles observed by CALIOP during the 2007–2009 period. Although a quantitative comparison is inconclusive as the HSRL backscatter appears to be biased high by a factor of two compared to in situ observations collected in April 2008 during the ARCTAS campaign over the High Canadian Arctic, it is nonetheless able to successfully reproduce the shape of the backscatter vertical profiles measured during the campaign. In relative terms, CALIOP and HSRL agree as to the fraction of column-integrated backscatter found near the surface (0–1 km) in winter (70–73 %) and in the free troposphere (1–8 km) in spring (35–46 %).

The 6-year CALIOP extinction observations enabled us to map the spatial distribution of the pan-Arctic surface aerosol maximum during winter. At high Arctic latitudes ($> 69°$ N) near the surface, CALIOP extinctions exhibit a strong peak in December–March and a summer minimum in all Arctic sectors. The largest values in winter extinction maximum are centered over the central Russian Arctic. This is consistent with enhanced low-level transport of Eurasian pollution to the Arctic induced by meridional transport along the Siberian anticyclone. In the Low Arctic near the surface, extinctions over the Asian, European and North American sectors exhibit a summer maximum in addition to the winter maximum. The summer enhancements are due to transport of biomass burning aerosols from boreal forest fires. During summer, CALIOP extinctions display a sharp drop between 60° N and 70° N. This gradient is likely the result of enhanced wet deposition combined with reduced transport from midlatitudes as the polar front retreats poleward.

There is a progressive shift of the CALIOP extinction maximum with altitude, from January at 0–2 km, to March at 2–5 km, to April at 5–8 km. The springtime peak extinction in the middle and upper troposphere is consistent with increased isentropic transport of pollution exported from the boundary layer by midlatitude cyclones. Meridional transport is favored by blocking patterns, which maximize in January–March. The Asian sector shows the highest extinctions in the middle and upper troposphere as cyclones and blocking patterns become more frequent in spring, favoring the uplift and northward transport of pollution from East Asia. Enhanced mineral dust transport from the deserts of northern China and Mongolia could also be contributing.

Widespread agricultural fires in Russia and Kazakhstan took place during spring 2008, when CALIOP extinctions displayed anomalously high extinctions in the midtroposphere compared to the 2006–2012 seasonal mean. The highest extinction anomaly in the summer record is linked to the intense wildfires that broke out in western Russia in July 2010. A protracted period of below-average extinctions was observed from August 2009 through May 2010 in the low and middle troposphere, which we link to a persistent and strong negative Arctic Oscillation event.

Our understanding of the processes controlling the emissions, transport and deposition of aerosols over the Arctic remain highly uncertain. Indeed, several recent studies have highlighted very large differences among chemical transport models over the Arctic (Textor et al., 2006, 2007; Shindell et al., 2008). Removal processes (wet and dry deposition) are particularly poorly constrained over the Arctic, which results in the inability of models to reproduce the observed seasonality of aerosol concentrations and their individual components (Liu et al., 2011; Bourgeois and Bey, 2011). Our multiyear spatial and temporal distribution of CALIOP extinctions over the Arctic will provide a new tool to validate these processes in global models.

Acknowledgements. We acknowledge the NASA Langley Research Center Atmospheric Science Data Center for the CALIPSO data, and the Langley Aerosol Research Group Experiment (LARGE) for the ARCTAS data. We like to thank Environment Canada and NOAA for providing the in-situ aerosol data at Alert and Barrow. The authors would also like to thank Tad Anderson, Zhaoyan Liu and Anne Jefferson for their useful suggestions. We also want to thank two anonymous reviewers for their valuable suggestions that resulted in significant improvements to the manuscript. This work was supported by funding from the NASA Earth and Space Science Fellowship under award NNX11AL69H and by NASA award NNX08AQ07G.

Edited by: M. Kopacz

References

Anderson, B. E., Cofer, W. R., Bagwell, D. R., Barrick, J. W., Hudgins, C. H., and Brunke, K. E.: Airborne observations of aircraft aerosol emissions I: Total nonvolatile particle emission indices, Geophys. Res. Lett., 25, 1689–1692, doi:10.1029/98GL00063, 1998.

Anderson, T. L. and Ogren, J. A.: Determining aerosol radiative properties using the TSI 3563 integrating nephelometer, Aerosol Sci. Technol., 29, 57–69, doi:10.1080/02786829808965551, 1998.

Anderson, T. L., Charlson, R. J., Winker, D. M., Ogren, J. A., Holmén, K.: Mesoscale Variations of Tropospheric Aerosols, J. Atmos. Sci., 60, 119–136, doi:10.1175/1520-0469(2003)060<0119:MVOTA>2.0.CO;2, 2003.

Barrie, L. A.: Arctic air pollution: An overview of current knowledge, Atmos. Environ., 20, 643–663, 1986.

Barrie, L. A., Hoff, R. M., and Daggupaty, S. M.: The influence of mid-latitudinal pollution sources on haze in the Canadian Arctic, Atmos. Environ., 15, 1407–1419, doi:10.1016/0004-6981(81)90347-4, 1981.

Barrie, L. A., Olson, M. P., and Oikawa, K. K.: The flux of anthropogenic sulphur into the Arctic from mid-latitudes in 1979/80, Atmos. Environ., 23, 2505–2512, doi:10.1016/0004-6981(89)90262-X, 1989.

Bian, H., Colarco, P. R., Chin, M., Chen, G., Rodriguez, J. M., Liang, Q., Blake, D., Chu, D. A., da Silva, A., Darmenov, A. S., Diskin, G., Fuelberg, H. E., Huey, G., Kondo, Y., Nielsen, J. E., Pan, X., and Wisthaler, A.: Source attributions of pollution to the Western Arctic during the NASA ARCTAS field campaign, Atmos. Chem. Phys., 13, 4707–4721, doi:10.5194/acp-13-4707-2013, 2013.

Bourdages, L., Duck, T. J., Lesins, G., Drummond, J. R., and Eloranta, E. W.: Physical properties of High Arctic tropospheric particles during winter, Atmos. Chem. Phys., 9, 6881–6897, doi:10.5194/acp-9-6881-2009, 2009.

Bourgeois, Q. and Bey, I.: Pollution transport efficiency toward the Arctic: Sensitivity to aerosol scavenging and source regions, J. Geophys. Res., 116, D08213, doi:10.1029/2010JD015096, 2011.

Brock, C. A., Cozic, J., Bahreini, R., Froyd, K. D., Middlebrook, A. M., McComiskey, A., Brioude, J., Cooper, O. R., Stohl, A., Aikin, K. C., de Gouw, J. A., Fahey, D. W., Ferrare, R. A., Gao, R.-S., Gore, W., Holloway, J. S., Hübler, G., Jefferson, A., Lack, D. A., Lance, S., Moore, R. H., Murphy, D. M., Nenes, A., Novelli, P. C., Nowak, J. B., Ogren, J. A., Peischl, J., Pierce, R. B., Pilewskie, P., Quinn, P. K., Ryerson, T. B., Schmidt, K. S., Schwarz, J. P., Sodemann, H., Spackman, J. R., Stark, H., Thomson, D. S., Thornberry, T., Veres, P., Watts, L. A., Warneke, C., and Wollny, A. G.: Characteristics, sources, and transport of aerosols measured in spring 2008 during the aerosol, radiation, and cloud processes affecting Arctic Climate (ARCPAC) Project, Atmos. Chem. Phys., 11, 2423–2453, doi:10.5194/acp-11-2423-2011, 2011.

Browell, E. V., Hair, J. W., Butler, C. F., Grant, W. B., DeYoung, R. J., Fenn, M. A., Brackett, V. G., Clayton, M. B., Brasseur, L. A., Harper, D. B., Ridley, B. A., Klonecki, A. A., Hess, P. G., Emmons, L. K., Tie, X., Atlas, E. L., Cantrell, C. A., Wimmers, A. J., Blake, D. R., Coffey, M. T., Hannigan, J. W., Dibb, J. E., Talbot, R. W., Flocke, F., Weinheimer, A. J., Fried, A., Wert, B., Snow, J. A., and Lefer, B. L.: Ozone, aerosol, potential vorticity, and trace gas trends observed at high-latitudes over North America from February to May 2000, J. Geophys. Res., 108, 8369, doi:10.1029/2001JD001390, 2003.

Browse, J., Carslaw, K. S., Arnold, S. R., Pringle, K., and Boucher, O.: The scavenging processes controlling the seasonal cycle in Arctic sulphate and black carbon aerosol, Atmos. Chem. Phys., 12, 6775–6798, doi:10.5194/acp-12-6775-2012, 2012.

Burton, S. P., Ferrare, R. A., Hostetler, C. A., Hair, J. W., Rogers, R. R., Obland, M. D., Butler, C. F., Cook, A. L., Harper, D. B., and Froyd, K. D.: Aerosol classification using airborne High Spectral Resolution Lidar measurements – methodology and examples, Atmos. Meas. Tech., 5, 73–98, doi:10.5194/amt-5-73-2012, 2012.

Carlson, T. N.: Speculations on the movement of polluted air to the Arctic, Atmos. Environ., 15, 1473–1477, doi:10.1016/0004-6981(81)90354-1, 1981.

Chen, S.-J., Kuo, Y.-H., Zhang, P.-Z., and Bai, Q.-F.: Synoptic Climatology of Cyclogenesis over East Asia, 1958–1987, Am. Meteor. Soc., 119, 1407–1418, doi:10.1175/1520-0493(1991)119<1407:SCOCOE>2.0.CO;2, 1991.

Clarke, A. D., Shinozuka, Y., Kapustin, V. N., Howell, S., Huebert, B., Doherty, S., Anderson, T., Covert, D., Anderson, J., Hua, X., Moore II, K. G., McNaughton, C., Carmichael, G., and Weber, R.: Size distributions and mixtures of dust and black carbon aerosol in Asian outflow: Physiochemistry and optical properties, J. Geophys. Res., 109, D15S09, doi:10.1029/2003JD004378, 2004.

Cohen, J., Foster, J., Barlow, M., Saito, K., and Jones, J.: Winter 2009–2010: A case study of an extreme Arctic Oscillation event, Geophys. Res. Lett., 37, L17707, doi:10.1029/2010GL044256, 2010.

Delene, D. J. and Ogren, J. A.: Variability of Aerosol Optical Properties at Four North American Surface Monitoring Sites, J. Atmos. Sci.,59(6), 1135–1150, doi:10.1175/1520-0469(2002)059<1135:VOAOPA>2.0.CO;2, 2002.

Devasthale, A., Tjernstrom, M., and Omar, A. H.: The vertical distribution of thin features over the Arctic analysed from CALIPSO observations, Tellus, 63B, 86–95, doi:10.1111/j.1600-0889.2010.00517.x, 2011.

de Villiers, R. A., Ancellet, G., Pelon, J., Quennehen, B., Schwarzenboeck, A., Gayet, J. F., and Law, K. S.: Airborne measurements of aerosol optical properties related to early spring transport of mid-latitude sources into the Arctic, Atmos. Chem. Phys., 10, 5011–5030, doi:10.5194/acp-10-5011-2010, 2010.

Di Pierro, M., Jaeglé, L., and Anderson, T. L.: Satellite observations of aerosol transport from East Asia to the Arctic: Three case studies, Atmos. Chem. Phys., 11, 2225–2243, doi:10.5194/acp-11-2225-2011, 2011.

Duncan, B. N. and Bey, I.: A modeling study of the export pathways of pollution from Europe: Seasonal and interannual variations (1987–1997), J. Geophys. Res., 109, D08301, doi:10.1029/2003JD004079, 2004.

Eckhardt, S., Stohl, A., Beirle, S., Spichtinger, N., James, P., Forster, C., Junker, C., Wagner, T., Platt, U., and Jennings, S. G.: The North Atlantic Oscillation controls air pollution transport to the Arctic, Atmos. Chem. Phys., 3, 1769–1778, doi:10.5194/acp-3-

1769-2003, 2003.

Eloranta, E. W., Razenkov, I. A., and Garcia, J. P.: Arctic Observations with the University of Wisconsin High Spectral Resolution Lidar, in Reviewed and Revised Papers Presented at the 23rd International Laser Radar Conference, edited by: Nagasawa, C. and Sugimoto, N., 399–402, 2006.

Fisher, J. A., Jacob, D. J., Purdy, M. T., Kopacz, M., Le Sager, P., Carouge, C., Holmes, C. D., Yantosca, R. M., Batchelor, R. L., Strong, K., Diskin, G. S., Fuelberg, H. E., Holloway, J. S., Hyer, E. J., McMillan, W. W., Warner, J., Streets, D. G., Zhang, Q., Wang, Y., and Wu, S.: Source attribution and interannual variability of Arctic pollution in spring constrained by aircraft (ARCTAS, ARCPAC) and satellite (AIRS) observations of carbon monoxide, Atmos. Chem. Phys., 10, 977–996, doi:10.5194/acp-10-977-2010, 2010.

Fisher, J. A., Jacob, D. J., Wang, Q., Bahreini, R., Carouge, C. C., Cubison, M. J., Dibb, J. E., Diehl, T., Jimenez, J. L., Leibensperger, E. M., Lu, Z. F., Meinders, M. B. J., Pye, H. O. T., Quinn, P. K., Sharma, S., Streets, D. G., van Donkelaar, A., and Yantosca, R. M.: Sources, distribution, and acidity of sulfate-ammonium aerosol in the Arctic in winter-spring. Atmospheric Environment, 45, 7301–7318, doi:10.1016/j.atmosenv.2011.08.030, 2011.

Fuelberg, H. E., Harrigan, D. L., and Sessions, W.: A meteorological overview of the ARCTAS 2008 mission, Atmos. Chem. Phys., 10, 817–842, doi:10.5194/acp-10-817-2010, 2010.

Garrett, T. J., Brattström, S., Sharma, S., Worthy, D. E. J., and Novelli, P.: The role of scavenging in the seasonal transport of black carbon and sulfate to the Arctic, Geophys. Res. Lett., 38, L16805, doi:10.1029/2011GL048221, 2011.

Gassó, S., Hegg, D. A., Covert, D. S., Collins, D., Noone, K. J., Öström, E., Schmid, B., Russell, P. B., Livingston, J. M., Durkee, P. A., and Jonsson, H.: Influence of humidity on the aerosol scattering coefficient and its effect on the upwelling radiance during ACE-2, Tellus, 52B, 546–567, doi:10.1034/j.1600-0889.2000.00055.x, 2000.

Gayet, J.-F., Mioche, G., Dörnbrack, A., Ehrlich, A., Lampert, A., and Wendisch, M.: Microphysical and optical properties of Arctic mixed-phase clouds. The 9 April 2007 case study., Atmos. Chem. Phys., 9, 6581–6595, doi:10.5194/acp-9-6581-2009, 2009.

Giglio, L., Csiszar, I., and Justice, C. O.: Global distribution and seasonality of active fires as observed with the Terra and Aqua Moderate Resolution Imaging Spectroradiometer (MODIS) sensors, J. Geophys. Res., 111, G02016, doi:10.1029/2005JG000142, 2006.

Gong, S. L., Zhao, T. L., Sharma, S., Toom-Sauntry, D., Lavoué, D., Zhang, X. B., Leaitch, W. R., and Barrie, L. A.: Identification of trends and interannual variability of sulfate and black carbon in the Canadian High Arctic: 1981–2007, J. Geophys. Res., 115, D07305, doi:10.1029/2009JD012943, 2010.

Grenier, P., Blanchet, J., and Muñoz-Alpizar, R.: Study of polar thin ice clouds and aerosols seen by CloudSat and CALIPSO during midwinter 2007, J. Geophys. Res., 114, D09201, doi:10.1029/2008JD010927, 2009.

Hegg, D. A., Warren, S. G., Grenfell, T. C., Doherty, S. J., and Clarke, A. D.: Sources of light-absorbing aerosol in arctic snow and their seasonal variation, Atmos. Chem. Phys., 10, 10923–10938, doi:10.5194/acp-10-10923-2010, 2010.

Heintzenberg, J., Birmili, W., Otto, R., Andreae, M. O., Mayer, J.-C., Chi, X., and Panov, A.: Aerosol particle number size distributions and particulate light absorption at the ZOTTO tall tower (Siberia), 2006–2009, Atmos. Chem. Phys., 11, 8703–8719, doi:10.5194/acp-11-8703-2011, 2011.

Hirdman, D., Burkhart, J. F., Sodemann, H., Eckhardt, S., Jefferson, A., Quinn, P. K., Sharma, S., Ström, J., and Stohl, A.: Long-term trends of black carbon and sulphate aerosol in the Arctic: changes in atmospheric transport and source region emissions, Atmos. Chem. Phys., 10, 9351–9368, doi:10.5194/acp-10-9351-2010, 2010.

Hoff, R. M.: Vertical Structure of Arctic Haze Observed by Lidar, J. Appl. Meteorol., 27, 125–139, doi:10.1175/1520-0450(1988)027<0125:VSOAHO>2.0.CO;2, 1988.

Ichoku, C., Giglio, L., Wooster, M. J., and Remner, L.: Global characterization of biomass-burning patterns using satellite measurements of fire radiative energy, Remote Sens. Environ., 112, 2950–2962, 2008.

Intrieri, J. M. and Shupe, M. D.: Characteristics and radiative effects of diamond dust over the Western Arctic Ocean region, J. Climate, 17, 2953–2960, doi:10.1175/1520-0442(2004)017<2953:CAREOD>2.0.CO;2, 2004.

Ishii, S., Shibata, T., Sakai, T., Kido, M., Hara, K., Osada, K., Iwasaka, Y., Nagai, T., Fujimoto, T., Itabe, T., Mizutani, K., and Uchino, O.: The source, size and chemical composition of the winter Arctic tropospheric aerosol layer observed by lidar at Eureka, Canada, J. Meteorol. Soc. Jpn., 79, 61–78, doi:10.2151/jmsj.79.61, 2001.

Iversen, T.: On the atmospheric transport of pollution to the Arctic, Geophys. Res. Lett, 11, 457–460, doi:10.1029/GL011i005p00457, 1984.

Iversen, T. and Joranger, E.: Arctic air pollution and large-scale atmospheric flows, Atmos. Environ., 19, 2099–2108, doi:10.1016/0004-6981(85)90117-9, 1985.

Jacob, D. J., Crawford, J. H., Maring, H., Clarke, A. D., Dibb, J. E., Emmons, L. K., Ferrare, R. A., Hostetler, C. A., Russell, P. B., Singh, H. B., Thompson, A. M., Shaw, G. E., McCauley, E., Pederson, J. R., and Fisher, J. A.: The Arctic Research of the Composition of the Troposphere from Aircraft and Satellites (ARCTAS) mission: design, execution, and first results, Atmos. Chem. Phys., 10, 5191–5212, doi:10.5194/acp-10-5191-2010, 2010.

Klein, W. H.: The frequency of cyclones and anticyclones in relation to the mean circulation, J. of Meteo., 15, 98–102, doi:10.1175/1520-0469(1958)015<0098:TFOCAA>2.0.CO;2, 1958.

Klonecki, A., Hess, P., Emmons, L., Smith, L., Orlando, J., and Blake, D.: Seasonal changes in the transport of pollutants into the Arctic troposphere-model study, J. Geophys. Res., 108, 8367, doi:10.1029/2002JD002199, 2003.

Koffi, B., Schulz, M., Bréon, F-M, Griesfeller, J., Winker, D. M., Balkanski, Y., Bauer, S., Berntsen, T., Chin, M., Collins, W. D., Dentener, F., Diehl, T., Easter, R. C., Ghan, S. J., Ginoux, P. A., Gong, S., Horowitz, L. W., Iversen, T., Kirkevag, A., Koch, D., M., Krol, M., Myhre, G., Stier, P., and Takemura, T.: Application of the CALIOP layer product to evaluate the vertical distribution of aerosols estimated by global models: AeroCom phase I results, J. Geophys. Res., 117, D10201, doi:10.1029/2011JD016858, 2012.

Kravitz, B., Robock, A., Bourassa, A., Deshler, T., Wu, D., Mattis, I., Finger, F., Hoffmann, A., Ritter, C., Bitar, L., Duck, T. J., and Barnes, J. E.: Simulation and observations of stratospheric aerosols from the 2009 Sarychev volcanic eruption, J. Geophys. Res., 116, D18211, doi:10.1029/2010JD015501, 2011.

Law, K. S. and Stohl, A.: Arctic air pollution: Origins and impacts, Science, 315, 1537–1540, doi:10.1126/science.1137695, 2007.

Lejenas, H. and Økland, H.: Characteristics of northern hemisphere blocking as determined from a long time series of observational data, Tellus, 35A, 350–362, 1983.

Liu, J., Fan, S., Horowitz, L. W., and Levy II, H.: Evaluation of factors controlling long-range transport of black carbon to the Arctic, J. Geophys. Res., 116, D04307, doi:10.1029/2010JD015145, 2011.

Liu, Z., Vaughan, M. A., Winker, D. M., Kittaka, C., Kuehn, R. E., Getzewich, B. J., Trepte, C. R., and Hostetler, C. A.: The CALIPSO Lidar Cloud and Aerosol Discrimination:Version 2 Algorithm and Initial Assessment of Performance, J. Atmos. Ocean. Technol., 26, 1198–1213, doi:10.1175/2009JTECHA1229.1, 2009.

Martinsson, B. G., Brenninkmeijer, C. A. M., Carn, S. A., Hermann, M., Heue, K.-P., van Velthoven, P. F. J., and Zahn, A.: Influence of the 2008 Kasatochi volcanic eruption on sulfurous and carbonaceous aerosol constituents in the lower stratosphere, Geophys. Res. Lett., 36, L12813, doi:10.1029/2009GL038735, 2009.

Matsui, H., Kondo, Y., Moteki, N., Takegawa, N., Sahu, L. K., Zhao, Y., Fuelberg, H. E., Sessions, W. R., Diskin, G., Blake, D. R., Wisthaler, A., and Koike, M.: Seasonal variation of the transport of black carbon aerosol from the asian continent to the Arctic during the ARCTAS aircraft campaign, J. Geophys. Res., 116, D05202, doi:10.1029/2010JD015067, 2011.

McConnell, J. R., Edwards, R., Kok, G. L., Flanner, M. G., Zender, C. S., Saltzman, E. S., Banta, J. R., Pasteris, D. R., Carter, M. M., and Kahl, J. D. W.: 20th-Century Industrial Black Carbon Emissions Altered Arctic Climate Forcing, Science, 317, 1381–1384, doi:10.1126/science.1144856, 2007.

Novakov, T., Ramanathan, V., Hansen, J. E., Kirchstetter, T. W., Sato, M., Sinton, J. E., and Satahye, J. A.: Large historical changes of fossil-fuel black carbon aerosols. Geophys. Res. Lett., 30, 1324, doi:10.1029/2002GL016345, 2003.

Omar, A. H, Winker, D. M., Kittaka, C., Vaughan, M. A., Liu, Z. Y., Hu, Y. X., Trepte, C. R., Rogers, R. R., Ferrare, R. A., Lee, K. P., Kuehn, R. E., and Hostetler, C. A.: The CALIPSO automated aerosol classification and lidar ratio selection algorithm, J. Atmos. Ocean. Technol., 26, 1994–2014, doi:10.1175/2009JTECHA1231.1, 2009.

Quinn, P. K., Miller, T. L., Bates, T. S., Ogren, J. A., Andrews, E., and Shaw, G. E.: A three year record of simultaneously measured aerosol chemical and optical properties at Barrow, Alaska, J. Geophys. Res., 107, 4130, doi:10.1029/2001JD001248, 2002.

Quinn, P. K., Shaw, G. E., Andrews, E., Dutton, E. G., Ruoho-Airola, T., and Gong, S. L.: Arctic haze: Current trends and knowledge gaps, Tellus, 59B, 99–114, doi:10.1111/j.1600-0889.2006.00238.x, 2007.

Quinn, P. K., Bates, T. S., Schulz, K., and Shaw, G. E.: Decadal trends in aerosol chemical composition at Barrow, Alaska: 1976–2008, Atmos. Chem. Phys., 9, 8883-8888, doi:10.5194/acp-9-8883-2009, 2009.

Raatz, W. and Shaw, G. E.: Long-range tropospheric transport of pollution aerosols into the Alsakan Arctic, J. Clim. Appl. Meteorol., 23, 1052–1064, 1984.

Rahn, K. A.: The Mn/V ratio as a tracer of large-scale sources of pollution aerosol for the Arctic, Atmos. Environ., 15, 1457–1464, doi:10.1016/0004-6981(81)90352-8, 1981.

Rahn, K. A. and Lowenthal, D. H.: Elemental tracers of distant regional pollution aerosols, Science, 223, 132–139, doi:10.1126/science.223.4632.132, 1984.

Rahn, K. A. and McCaffrey, R. J.: On the origin and transport of the winter Arctic aerosol, Ann. N. Y. Acad. Sci., 338, 486–503, 1980.

Rahn, K. A., Borys, R. D., and Shaw, G. E.: Asian source of Arctic haze bands, Nature, 268, 713–715, 1977.

Rogers, R. R., Hostetler, C. A., Hair, J. W., Ferrare, R. A., Liu, Z., Obland, M. D., Harper, D. B., Cook, A. L., Powell, K. A., Vaughan, M. A., and Winker D. M.: Assessment of the CALIPSO Lidar 532nm attenuated backscatter calibration using the NASA LaRC airborne High Spectral Resolution Lidar, Atmos. Chem. Phys., 11, 1295–1311, doi:10.5194/acp-11-1295-2011, 2011.

Scheuer, E., Talbot, R. W., Dibb, J. E., Seid, G. K., DeBell, L., and Lefer, B.: Seasonal distributions of fine aerosol sulfate in the North American Arctic basin during TOPSE, J. Geophys. Res., 108, 8370, doi:10.1029/2001JD001364, 2003.

Schmale, J., Schneider, J., Ancellet, G., Quennehen, B., Stohl, A., Sodemann, H., Burkhart, J. F., Hamburger, T., Arnold, S. R., Schwarzenboeck, A., Borrmann, S., and Law, K. S.: Source identification and airborne chemical characterisation of aerosol pollution from long-range transport over Greenland during POLARCAT summer campaign 2008, Atmos. Chem. Phys., 11, 10097-10123, doi:10.5194/acp-11-10097-2011, 2011.

Seager, R., Kushnir, Y., Nakamura, J., Ting, M., and Naik, N.: Northern Hemisphere winter snow anomalies: ENSO, NAO and the winter of 2009/10, Geophys. Res. Lett., 37, L14703, doi:10.1029/2010GL043830, 2010.

Shao, Y. and Dong, C. H.: A review on East Asian dust storm climate, modeling and monitoring, Global Planet. Change, 52, 1–22, 2006.

Shaw, G. E.: The Arctic Haze phenomenon, B. Am. Meteor. Soc., 76, 2403–2413, doi:10.1175/1520-0477(1995)076<2403:TAHP>2.0.CO;2, 1995.

Shindell, D. T., Chin, M., Dentener, F., Doherty, R. M., Faluvegi, G., Fiore, A. M., Hess, P., Koch, D. M., MacKenzie, I. A., Sanderson, M. G., Schultz, M. G., Schulz, M., Stevenson, D. S., Teich, H., Textor, C., Wild, O., Bergmann, D. J., Bey, I., Bian, H., Cuvelier, C., Duncan, B. N., Folberth, G., Horowitz, L. J., Kaminski, J. W., Marmer, E., Park, R., Pringle, K. J., Schroeder, S., Szopa, S., Takemura, T., Zeng, G., Keating, T. J., and Zuber, A.: A multi-model assessment of pollution transport to the Arctic, Atmos. Chem. Phys., 8, 5353–5372, doi:10.5194/acp-8-5353-2008, 2008.

Shinozuka, Y., Redemann, J., Livingston, J. M., Russell, P. B., Clarke, A. D., Howell, S. G., Freitag, S., O'Neill, N. T., Reid, E. A., Johnson, R., Ramachandran, S., McNaughton, C. S., Kapustin, V. N., Brekhovskikh, V., Holben, B. N., and McArthur, L. J. B.: Airborne observation of aerosol optical depth during ARCTAS: vertical profiles, inter-comparison and fine-mode fraction, Atmos. Chem. Phys., 11, 3673–3688, doi:10.5194/acp-11-3673-2011, 2011.

Stern, D. I.: Global sulfur emissions from 1850 to 2000, Chemosphere, 58, 163–175, doi:10.1016/j.chemosphere.2004.08.022, 2005.

Stohl, A.: Characteristics of atmospheric transport into the Arctic troposphere, J. Geophys. Res., 111, D11306, doi:10.1029/2005JD006888, 2006.

Stohl, A., Eckhardt, S., Forster, C., James, P., and Spichtinger, N.: On the pathways and timescales of intercontinental air pollution transport, J. Geophys. Res., 107, 4684, doi:10.1029/2001JD001396, 2002.

Sun, J., Zhang, M., and Liu, T.: Spatial and temporal characteristics of dust storms in China and its surrounding regions, 1960–1999: Relations to source area and climate, J. Geophys. Res., 106, 10325–10333, doi:10.1029/2000JD900665, 2001.

Textor, C., Schulz, M., Guibert, S., Kinne, S., Balkanski, Y., Bauer, S., Berntsen, T., Berglen, T., Boucher, O., Chin, M., Dentener, F., Diehl, T., Easter, R., Feichter, H., Fillmore, D., Ghan, S., Ginoux, P., Gong, S., Grini, A., Hendricks, J., Horowitz, L., Huang, P., Isaksen, I., Iversen, I., Kloster, S., Koch, D., Kirkevåg, A., Kristjansson, J. E., Krol, M., Lauer, A., Lamarque, J. F., Liu, X., Montanaro, V., Myhre, G., Penner, J., Pitari, G., Reddy, S., Seland, Ø., Stier, P., Takemura, T., and Tie, X.: Analysis and quantification of the diversities of aerosol life cycles within AeroCom, Atmos. Chem. Phys., 6, 1777–1813, doi:10.5194/acp-6-1777-2006, 2006.

Textor, C., Schulz, M., Guibert, S., Kinne, S., Balkanski, Y., Bauer, S., Berntsen, T., Berglen, T., Boucher, O., Chin, M., Dentener, F., Diehl, T., Feichter, J., Fillmore, D., Ginoux, P., Gong, S., Grini, A., Hendricks, J., Horowitz, L., Huang, P., Isaksen, I. S. A., Iversen, T., Kloster, S., Koch, D., Kirkevåg, A., Kristjansson, J. E., Krol, M., Lauer, A., Lamarque, J. F., Liu, X., Montanaro, V., Myhre, G., Penner, J. E., Pitari, G., Reddy, M. S., Seland, Ø., Stier, P., Takemura, T., and Tie, X.: The effect of harmonized emissions on aerosol properties in global models – an AeroCom experiment, Atmos. Chem. Phys., 7, 4489–4501, doi:10.5194/acp-7-4489-2007, 2007.

Treffeisen, R. E., Thomason, L. W. , Ström, J., Herber, A. B., Burton, S. P., and Yamanouchi, T.: Stratospheric Aerosol and Gas Experiment (SAGE) II and III aerosol extinction measurements in the Arctic middle and upper troposphere, J. Geophys. Res., 111, D17203, doi:10.1029/2005JD006271, 2006.

Val Martin, M., Logan, J. A., Kahn, R. A., Leung, F.-Y., Nelson, D. L., and Diner, D. J.: Smoke injection heights from fires in North America: analysis of 5 years of satellite observations, Atmos. Chem. Phys., 10, 1491–1510, doi:10.5194/acp-10-1491-2010, 2010.

van der Werf, G. R., Randerson, J. T., Giglio, L., Collatz, G. J., Kasibhatla, P. S., and Arellano Jr., A. F.: Interannual variability in global biomass burning emissions from 1997 to 2004, Atmos. Chem. Phys., 6, 3423–3441, doi:10.5194/acp-6-3423-2006, 2006.

Wang, Q., Jacob, D. J., Fisher, J. A., Mao, J., Leibensperger, E. M., Carouge, C. C., Le Sager, P., Kondo, Y., Jimenez, J. L., Cubison, M. J., and Doherty, S. J.: Sources of carbonaceous aerosols and deposited black carbon in the Arctic in winter-spring: implications for radiative forcing, Atmos. Chem. Phys., 11, 12453–12473, doi:10.5194/acp-11-12453-2011, 2011.

Warneke, C., Bahreini, R., Brioude, J., Brock, C. A., de Gouw, J. A., Fahey, D. W., Froyd, K. D., Holloway, J. S., Middlebrook, A., Miller, L., Montzka, S., Murphy, D. M., Peischl, J., Ryerson, T. B., Schwarz, J. P., Spackman, J. R., and Veres, P.: Biomass burning in Siberia and Kazakhstan as an important source for haze over the Alaskan Arctic in April 2008, Geophys. Res. Lett., 36, L02813, doi:10.1029/2008GL036194, 2009.

Warneke, C., Froyd, K. D., Brioude, J., Bahreini, R., Brock, C. A., Cozic, J., de Gouw, J. A., Fahey, D. W., Ferrare, R., Holloway, J. S., Middlebrook, A. M., Miller, L., Montzka, S., Schwarz, J. P., Sodemann, H., Spackman, J. R., and Stohl, A.: An important contribution to springtime Arctic aerosol from biomass burning in Russia, Geophys. Res. Lett., 37, L01801, doi:10.1029/2009GL041816, 2010.

Winker, D. M., Vaughan, M. A., Omar, A., Hu, Y., and Powell, J. A.: Overview of the CALIPSO Mission and CALIOP Data Processing Algorithms, J. Atmos. Ocean. Technol., 26, 2310–2323, doi:10.1175/2009JTECHA1281.1, 2009.

Winker, D. M., Tackett, J. L., Getzewich, B. J., Liu, Z., Vaughan, M. A., and Rogers, R. R.: The global 3-D distribution of tropospheric aerosols as characterized by CALIOP, Atmos. Chem. Phys., 13, 3345–3361, doi:10.5194/acp-13-3345-2013, 2013.

Witte, J. C., Douglass, A. R., da Silva, A., Torres, O., Levy, R., and Duncan, B. N.: NASA A-Train and Terra observations of the 2010 Russian wildfires, Atmos. Chem. Phys., 11, 9287–9301, doi:10.5194/acp-11-9287-2011, 2011.

Young, S. A. and Vaughan, M. A.: The retrieval of profiles of particulate extinction from Cloud Aerosol Lidar Infrared Pathfinder Satellite Observations (CALIPSO) data: Algorithm description, J. Atmos. Ocean. Tech., 26, 1105–1119, doi:10.1175/2008JTECHA1221.1, 2009.

Yu, H., Chin, M., Winker, D. M., Omar, A. H., Liu, Z., Kittaka, C., and Diehl, T.: Global view of aerosol vertical distributions from CALIPSO lidar measurements and GOCART simulations: Regional and seasonal variations, J. Geophys. Res., 115, D00H30, doi:10.1029/2009JD013364, 2010.

Yumimoto, K., Eguchi, K., Uno, I., Takemura, T., Liu, Z., Shimizu, A., and Sugimoto, N.: An elevated large-scale dust veil from the Taklimakan Desert: Intercontinental transport and three-dimensional structure as captured by CALIPSO and regional and global models, Atmos. Chem. Phys., 9, 8545–8558, doi:10.5194/acp-9-8545-2009, 2009.